

4

AFGL-TR-88-0054

DTIC FILE COPY

The Discrimination Potential of Crustal  
Resonance Phases

L.J. Burdick  
D.V. Helmberger

Woodward-Clyde Consultants  
566 El Dorado Street  
Suite 100  
Pasadena, CA 91101

DTIC  
ELECTE  
JUN 27 1988  
S D

15 October 1987

Scientific Report No. 1

APPROVED FOR PUBLIC RELEASE; DISTRIBUTION UNLIMITED

AIR FORCE GEOPHYSICS LABORATORY  
AIR FORCE SYSTEMS COMMAND  
UNITED STATES AIR FORCE  
HANSCOM AIR FORCE BASE, MASSACHUSETTS 01731-5000

AD-A196 096


88 026

"This technical report has been reviewed and is approved for publication"

  
JAMES F. LEWKOWICZ  
Contract Manager

  
HENRY A. OSSING  
Branch Chief

FOR THE COMMANDER

  
DONALD H. ECKHARDT  
Division Director

This report has been reviewed by the ESD Public Affairs Office (PA) and is releasable to the National Technical Information Service (NTIS).

Qualified requestors may obtain additional copies from the Defense Technical Information Center. All others should apply to the National Technical Information Service.

If your address has changed, or if you wish to be removed from the mailing list, or if the addressee is no longer employed by your organization, please notify AFGL/DAA, Hanscom AFB, MA 01731. This will assist us in maintaining a current mailing list.

Do not return copies of this report unless contractual obligations or notices on a specific document requires that it be returned.

Unclassified

SECURITY CLASSIFICATION OF THIS PAGE

## REPORT DOCUMENTATION PAGE

1a REPORT SECURITY CLASSIFICATION Unclassified			1b RESTRICTIVE MARKINGS		
2a SECURITY CLASSIFICATION AUTHORITY			3 DISTRIBUTION / AVAILABILITY OF REPORT Approved for public release; distribution unlimited.		
2b DECLASSIFICATION / DOWNGRADING SCHEDULE					
4 PERFORMING ORGANIZATION REPORT NUMBER(S) WCCP-R-88-01			5 MONITORING ORGANIZATION REPORT NUMBER(S) AFGL-TR-88-0054		
6a NAME OF PERFORMING ORGANIZATION Woodward-Clyde Consultants		6b OFFICE SYMBOL (If applicable)		7a NAME OF MONITORING ORGANIZATION Air Force Geophysics Laboratory	
6c ADDRESS (City, State, and ZIP Code) 566 El Dorado Street, Suite 100 Pasadena, CA 91101			7b ADDRESS (City, State, and ZIP Code) Hanscom Air Force Base Massachusetts 01731-5000		
8a NAME OF FUNDING / SPONSORING ORGANIZATION DARPA		8b OFFICE SYMBOL (If applicable)		9 PROCUREMENT INSTRUMENT IDENTIFICATION NUMBER F19628-87-C-0081	
8c ADDRESS (City, State, and ZIP Code) 1400 Wilson Boulevard Arlington, VA 22209			10 SOURCE OF FUNDING NUMBERS		
			PROGRAM ELEMENT NO 62714E	PROJECT NO 7A10	TASK NO DA
			WORK UNIT ACCESSION NO DD		
11 TITLE (Include Security Classification) The Discrimination Potential of Crustal Resonance Phases (Unclassified)					
12 PERSONAL AUTHOR(S) L. J. Burdick and D. V. Helmberger					
13a TYPE OF REPORT Scientific Report #1		13b TIME COVERED FROM 3/5/87 TO 9/5/87		14 DATE OF REPORT (Year, Month, Day) 1987 October 15	
15 PAGE COUNT 96					
16 SUPPLEMENTARY NOTATION					
17 COSATI CODES			18 SUBJECT TERMS (Continue on reverse if necessary and identify by block number)		
FIELD	GROUP	SUB-GROUP	Regional Discriminants, P <sub>g</sub> , P <sub>n1</sub> , Synthetic Seismograms		
19 ABSTRACT (Continue on reverse if necessary and identify by block number)  See Reverse Side of Page					
20 DISTRIBUTION / AVAILABILITY OF ABSTRACT <input checked="" type="checkbox"/> UNCLASSIFIED/UNLIMITED <input type="checkbox"/> SAME AS RPT <input type="checkbox"/> DTIC USERS			21 ABSTRACT SECURITY CLASSIFICATION Unclassified		
22a NAME OF RESPONSIBLE INDIVIDUAL James Lewkowicz			22b TELEPHONE (Include Area Code) (617) 377-3028		22c OFFICE SYMBOL AFGL/LWH

## BLOCK 19: ABSTRACT

→ It is unlikely that regional data recorded at a newly installed array of stations could be used immediately to reliably discriminate events because of uncertainties about the local characteristics of wave propagation. However, the stations would immediately begin to record  $P_{nl}$  data from small local events. This raises the possibility that the earthquake data base could be used to calibrate the array for discrimination purposes. To investigate this possibility, we have begun to study the relationships between long period  $P_{nl}$  data and high frequency regional phases in the western U. S. In this report we examine the phase  $P_s$ . The high frequency  $P_s$  phase for small, shallow events typically appears as a complex arrival with a duration of several tens of seconds. This is much longer than the possible duration of the effective source time function even with depth phases taken into account. This phenomenon can be explained by synthesizing  $P_s$  using generalized rays which is a practical computational procedure for a simple layer over a half space crustal model. If model responses are computed by progressively adding in rays with one reverberation in the crust, then two and so on, it is observed that a sequence of high frequency arrivals develops spanning the typical duration of  $P_s$ . Each successive resonance phase is associated with a higher order reverberation in the crust. If each arrival contributes a typical amount of high frequency scattered energy, the long duration of  $P_s$  is simple to understand. Though there are over a thousand generalized rays which must be summed to generate the first 5 crustal reverberations, only a few of them contribute strongly to each resonance phase. The first is dominated by  $PmP$ ,  $SmS$  and their depth phases, and the second is dominated by the converted phases associated with the first reverberation. This may have strong implications in efforts to improve source discrimination capabilities, since source depth and excitation of shear energy are the primary differences between explosions and earthquakes. To investigate the stability of these crustal resonances, profiles of regional long period records for NTS explosions and a moderate sized Nevada earthquake were collected and modeled. The crustal resonance phases appear to be stable and deterministic down to periods of 1 or 2 s. → The implication is that the arrival times of synthetic crustal resonance phases may be used as a guide in selecting windows of time in the long  $P_s$  coda when information rich in discrimination potential is arriving. (See Appendix, p. 16)

# TABLE OF CONTENTS

	PAGE
Introduction	1
Broad Band Regional Records in the Western United States	4
Regional Wave Propagation in the Western United States	11
Crustal Resonance Phases	22
Observations and Models of Crustal Resonance Phases	30
Improved Methods for Computing $P_{n1}$	56
Discussion	70
Conclusions	72
References	73



Answer For	
NTIS CRA&I	<input checked="" type="checkbox"/>
DTIC TAB	<input type="checkbox"/>
Unannounced	<input type="checkbox"/>
Justification	
Availability Codes	
A-1	

## INTRODUCTION

The focus of research in discrimination in recent years has shifted toward the development of techniques based on high frequency regional phases. This has occurred because it has become apparent that long period discriminants will always suffer from uncertainties due to tectonic release and because decoupling is believed to be more efficient at long periods. The shift to regional rather than teleseismic phases is necessitated by the fact that very small events will need to be identified to monitor a low threshold or total test ban treaty. Research in this area has consisted almost entirely of the development of empirical and semi-empirical methods of separating earthquakes from explosions using high frequency data alone. Pomeroy et al. (1982) have reviewed these efforts and report that, as yet, no highly successful discriminant has been found. Moreover, those discriminants that appear to perform reliably under one geographic set of circumstances fail in others. The spectral discriminant of Murphy and Bennett (1982) is one good example of this (Blandford, 1982). The fundamental idea behind the research being performed in this effort is that the longer period information recorded at a site, even though it is not used for discrimination itself, can be used to calibrate regional discriminants.

It can be anticipated that when a regional station is installed at a new site the potential for discriminating events using data from it will be relatively low. However, it will begin to record broadband signals from regional events almost immediately. Most of these events will be reliably identified as earthquakes or explosions using current discrimination

technology. In this study, we demonstrate how the signals from these local events can be used to establish the characteristics of regional wave propagation that most influence discrimination procedures. As the signals from these events are analyzed, regional discriminants will become better calibrated and the data from the station will increase in importance with regard to discrimination. The procedure might be described as bootstrapping the accuracy of a regional discrimination methodology.

In this, the initial phase of the work, we have worked with regional signals at stations in the western U.S. Because of the long history of intense seismological study of this area, we have the results of many previous studies to draw on. Those of most importance in this work are those of long period  $P_{n1}$  waves initiated by Helmberger and Engen (1980) and followed by Wallace et al. (1981, 1983). The term  $P_{n1}$  wave refers to the long period signal arriving in about the first one to two minutes of the P wave. The onset would be described as the classical  $P_n$  wave, and it is followed by the long period  $P_l$  wave which moves at a substantially slower velocity. The composite signal is  $P_{n1}$ . The phase turns out to be remarkably stable so that it can be easily modeled to high accuracy. In general, it is a long period signal, and it is of no direct use to solving the high frequency discrimination problem. But the result of a program of long period  $P_{n1}$  modeling is a capability of predicting for any observed high frequency signal a corresponding long period signal. This capability does not depend on how small the event causing the signal was. This synthetic long period signal can be used as an envelope of the much more complex high frequency signal to guide in how to most efficiently interpret it.

In this study, we have investigated how the  $P_{n1}$  envelope can be used to aid in discrimination analysis of high frequency  $P_g$  arrivals. We show that the  $P_g$  phase has an interesting substructure. It can be thought of as a series of arrivals which we have named crustal resonance phases. These subphases are composed of groups of rays with very similar travel times. Some of these groups of rays are dominated by depth phases, others by converted phases and still others by high order crustal multiples. It is reasonable to expect that those crustal resonances strongly influenced by depth phases or S to P converted energy will have a high discrimination potential.

We begin by showing some observed and theoretical examples of crustal resonance phases. Then we present a discussion of general regional body wave propagation in the western U S. We present observed and synthetic profiles of  $P_{n1}$  waves from NTS explosions and the nearby Caliente earthquake, and finally a discussion of how current methods of  $P_{n1}$  analysis needs to be generalized to enhance discrimination capabilities.



## BROAD BAND REGIONAL RECORDS IN THE WESTERN UNITED STATES

The events used in calibrating a regional station do not need to be large. As an example, let us consider a small event which occurred in Idaho on October 29, 1983 as it was recorded at the RSTN station RSSD. Its magnitude was only  $m_b=5.4$ , but it produced a good signal 800 km away as shown in Figure 1. The three components of motion are shown there for the long, intermediate and short period channels. These data illustrate of why it is important to use long period data to provide a structure within which short period data can be more fully understood. The station is naturally rotated with respect to the event, so that SH motion appears almost exclusively on the NS channel and P-SV energy on the EW and Z channels. In the long period records, the motions are consistent with a stratified earth structure. A clear P wave appears first on the Z and E channels while the first long period signal on the N channel is the SH which is followed by a simple Love wave. Thus the long period information can be interpreted using the powerful analytic tools appropriate for use in a stratified structure. In the intermediate channel, the particle motion is less well behaved. There is a small signal on the transverse component at the P arrival time which grows at the  $P_g$  arrival. There is still a distinct SH pulse followed by  $L_g$  and the Love wave. On the short period channel, the P signal appears with equal power on all components. The particle motion is completely inconsistent with a stratified velocity structure. Making discrimination decisions based on the incoherent signals in the short period band is very difficult. The more coherent energy from reference events in the other two bands needs to be utilized to the fullest possible extent in arriving at correct event discrimination.

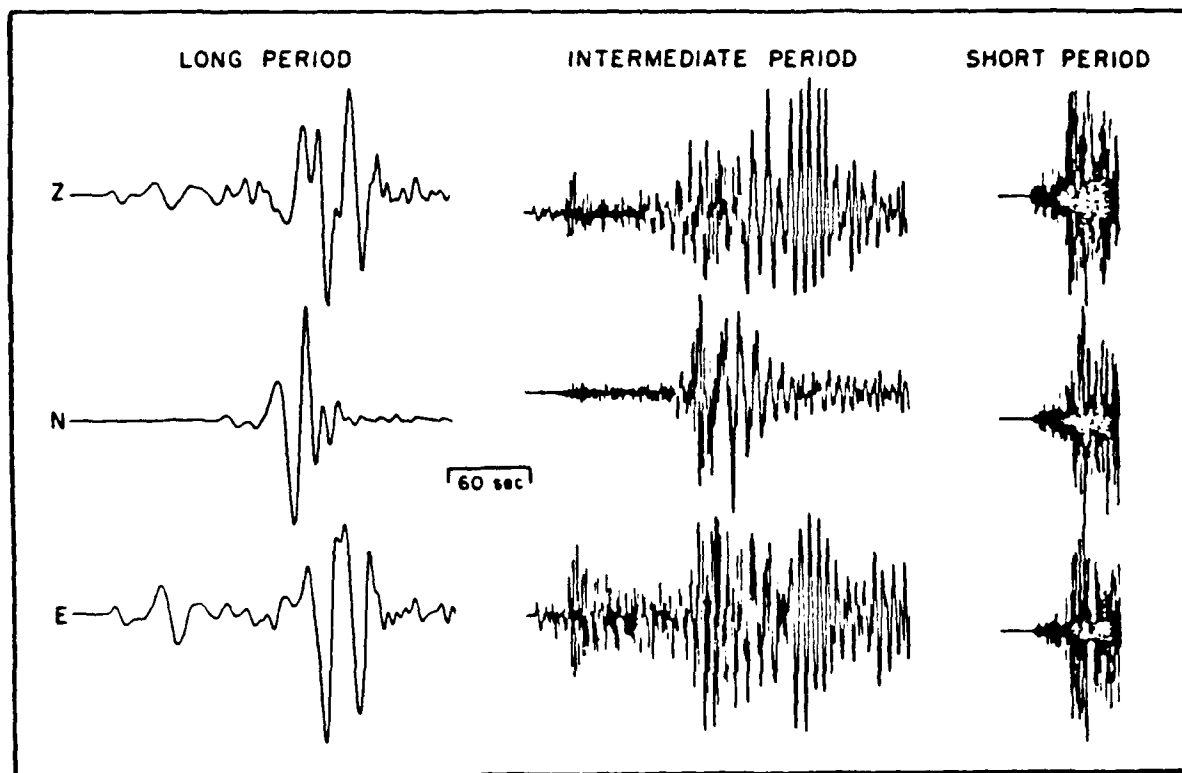


Figure 1. Three component observations of a small Idaho earthquake at station RSSD (range 700 km) in three different period bands.

One of the difficulties in relating information from long period signals to that in short period signals is that, because of the different physics controlling wave propagation in the two bands (coherent propagation in a layered medium vs semi-scattered or diffusive propagation), different nomenclatures have evolved for describing signals with the same arrival time in the two different bands. It is important for the purposes of this discussion to clarify some of this nomenclature.

The first 90 seconds of the vertical signals from Figure 1 are displayed in a column in Figure 2 on an expanded time scale. The long period signal shown at the top contains two clear pulses. The first is a classical  $P_n$  arrival, or a head wave propagating along the crust mantle interface. The second arrival is called a  $P_L$  wave and was first studied in detail by Oliver and Major (1960). It is generated by long period energy trapped and reverberating within the crust. PS type head waves also contribute strongly to the long period  $P_L$ . At the bottom of the figure is shown the short period signal which contains a large number of sub-arrivals. The first arriving energy is generally called  $P_n$ , but its relationship to the long period  $P_n$  arrival is relatively weak. As noted earlier, its particle motion is inconsistent with pure compressional motion, and its amplitude is also much too large as compared to theoretical predictions for a high frequency head wave. The large burst of energy on the short period channel about 50 s after the first arrival is generally called  $P_g$ . Its duration on the short period record is very much longer than the duration of the source or even the duration of the source and it's depth phases. It can be inferred from this that energy in the composite phase  $P_g$  must be traveling along very many different ray paths. It will probably be necessary to analyze it in terms of its sub-phases to properly understand it.

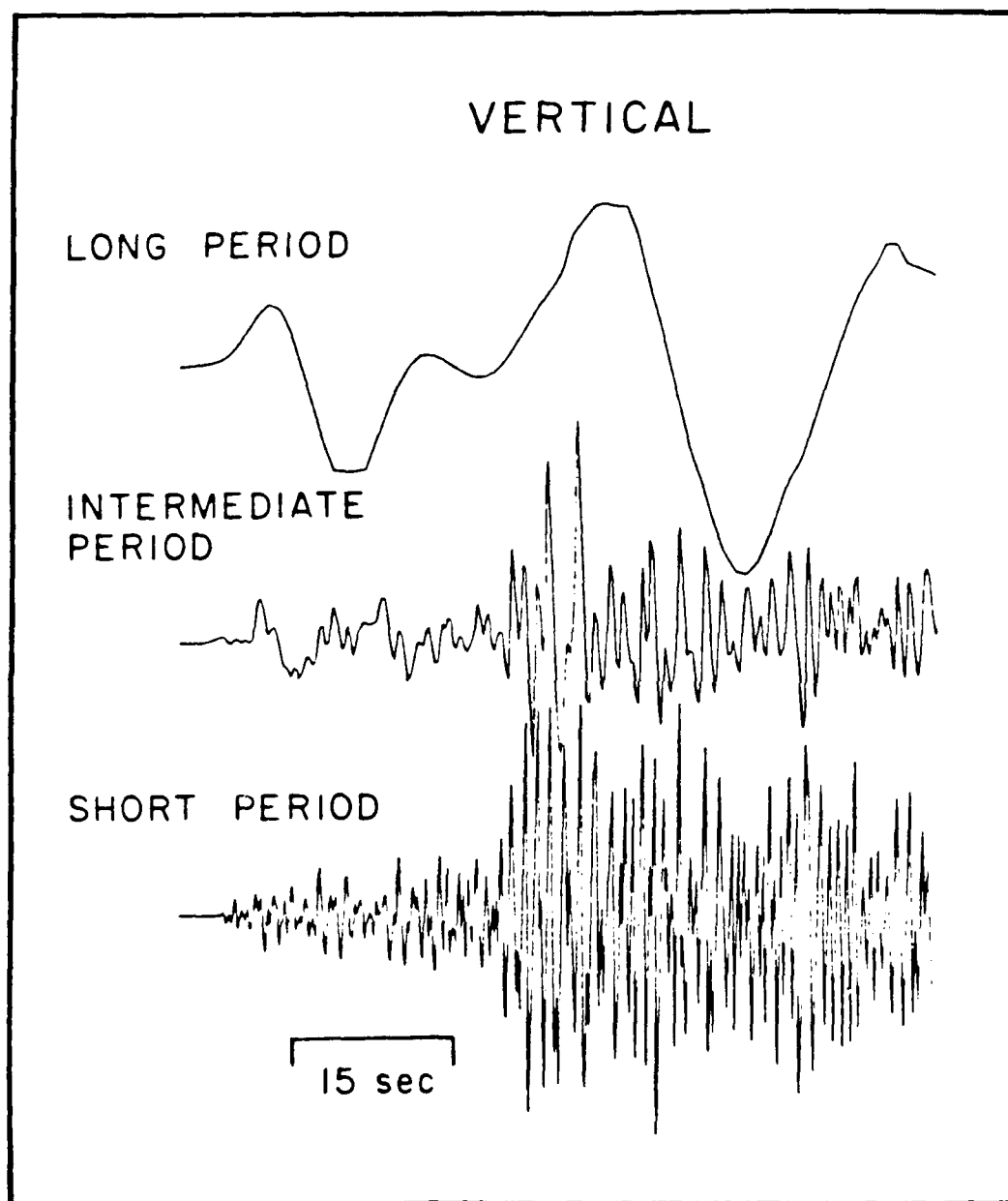


Figure 2. Vertical channel P waves from the small Idaho earthquake at RSSD displayed on the same time scale. The first arrival is  $P_n$  and the second is  $P_g$ .

Another name for another arrival that is often discussed in ray modeling studies of regional P waves is the phase PmP. This is the reflected arrival from the crust mantle transition. At ranges past the critical distance, it is the reflection associated with the  $P_n$  head wave. In an important study on western U.S. regional wave propagation, Langston and Helmberger (1974) demonstrated that the PmP arrival coincides with the beginning of  $P_g$ . In this work, we show that there is a close relationship between PmP and the onset of  $P_g$  and that understanding and exploiting this relationship might easily lead to enhanced discrimination capabilities.

Intermediate period data channels like those in the new digital stations have not been in operation for any great length of time. Thus there have not been many studies of data from them, and no separate nomenclature for phases observed on them has been developed. In this work, we introduce the "crustal resonance phase" which is perhaps best observed on this channel. Referring to the intermediate period data in Figure 2, we find that the  $P_n$  arrival appears relatively deterministic and is followed by moderate coda up to the  $P_g$  or PmP arrival. The first  $P_g$  appears to be made up of a series of heavily interfering pulses and is then followed by a series of resonance phases at about every 10 seconds. There are corresponding maxima in the envelope of the short period signal on the bottom. We will provide a possible interpretation of these resonances in following sections.

An appropriate technique for computing synthetic seismograms at regional ranges at long periods is the one presented by Helmberger and Engen (1980) for computing  $P_{nl}$  waves. In these calculations, the crust is represented as a uniform layer and its response is computed by summing large numbers of

generalized rays. Records from the intermediate channel of the RSTN are by no means long period and must certainly be sensitive to some of the detailed structure of the crust. Nonetheless, it is informative to compute synthetics using this approach. A comparison between the intermediate period vertical and radial records from RSSD and  $P_{n1}$  synthetics is shown in Figure 3. The mechanism of the event is unknown, but it is an aftershock of the October 28, 1983 Borah Peak event in eastern Idaho which had a normal mechanism. The synthetic shown in the figure is for a  $45^\circ$  dipping normal fault. The match of the  $P_n$  waveform is reasonable given the approximations which have been made. An initial two pulses are observed in the records and predicted in the synthetics though the first pulse is much smaller in the data than the synthetics. The synthetics also predict a series of resonance phases much like those observed in the data. At the beginning of the  $P_g$  or  $PmP$  arrival, the match is good enough to suggest that with some fine tuning of the crustal structure some deterministic modeling might be possible. In the following, we will discuss the origin of crustal resonances and explore the possibility of modeling them.

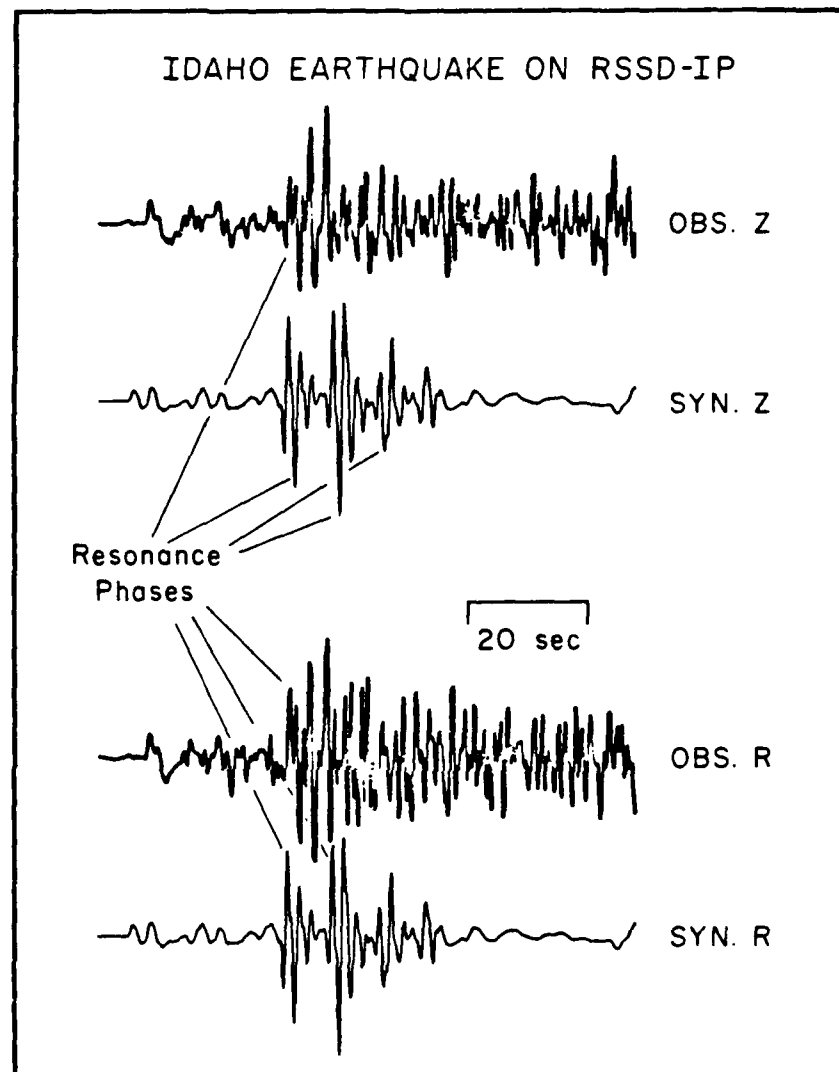


Figure 3. A comparison between observed and synthetic intermediate period P wave records from the small Idaho earthquake. The synthetics were computed using the methodology of Helmberger and Engen (1980). The arrivals we propose to call crustal resonance phases are indicated.

## REGIONAL WAVE PROPAGATION IN THE WESTERN UNITED STATES

Before commencing with further discussion of crustal resonance phases, it is appropriate to review the general subject of regional wave propagation in the western U.S. This will clarify why the layer over a half space,  $P_{n1}$  calculations of HelMBERGER and Engen (1980) are so relevant. It will also provide insight into how discrimination techniques developed in the western U.S. might need to be modified to be translated to other areas.

It has been shown in a series of studies that the  $P_{n1}$  formalism for computing synthetics is valid in the western U.S. for ranges beginning when the  $P_n$  crosses over to become the first arrival out to ranges of about 11 or 12°. This corresponds to about 150 to 1300 km. Because of the high seismicity rate and dense instrumentation of the area, there have been many earth structure studies carried out there over time including refraction surveys (Pakiser, 1963), modeling studies of the lid and low velocity zone (HelMBERGER, 1973) and modeling studies of the upper mantle (Burdick and HelMBERGER, 1978). A composite model from several of these studies of the top 200 km of the earth is shown in Figure 4. The refraction surveys have shown that the crust has a relatively weak gradient and does not exhibit any consistent evidence for a mid-crustal or Conrad discontinuity. The uniform crustal layer shown in the figure is the one used by HelMBERGER and Engen (1980) for their calculations. Though the crust does undoubtedly have some velocity gradient, this will not have a large effect on body waves propagating almost vertically through it. This vertical propagation condition is satisfied at ranges past  $P_n$  crossover. The lid in the western U.S. has a weak



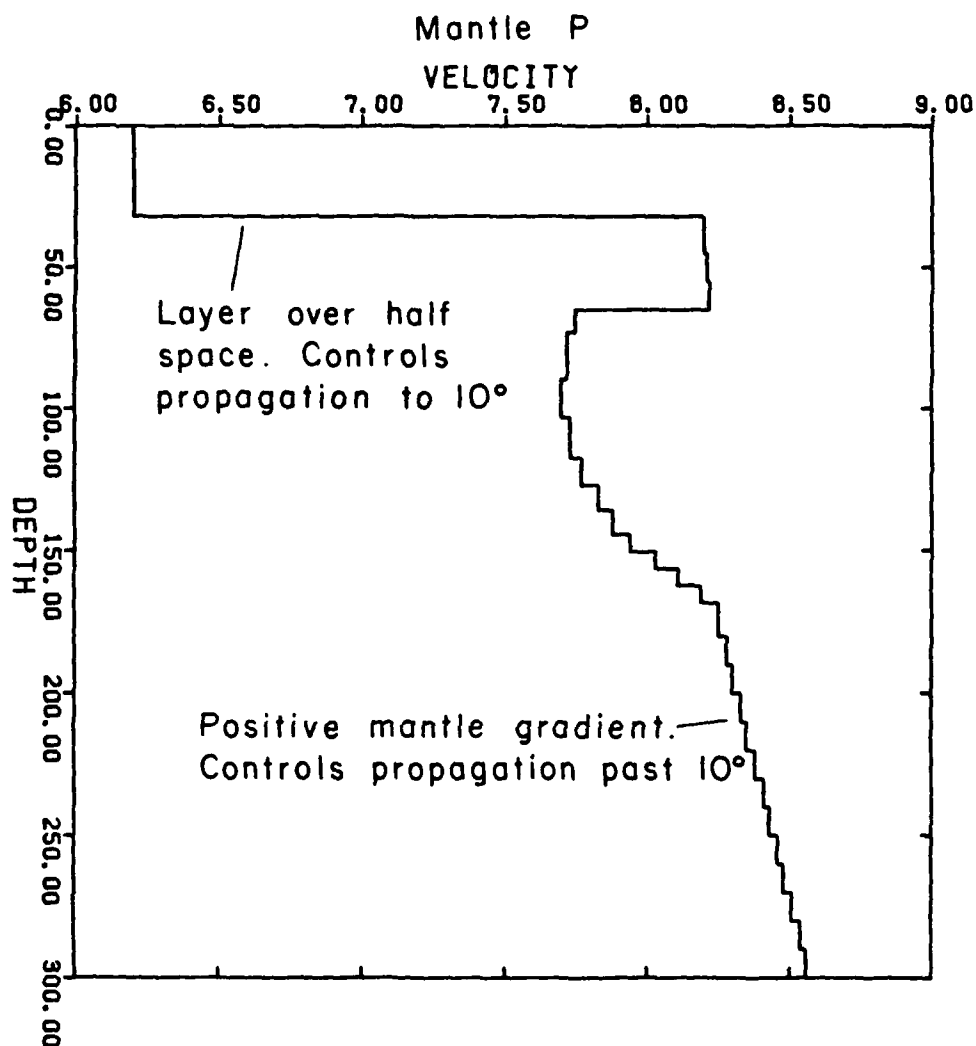


Figure 4. A realistic layered velocity model for the crust and upper mantle in the western U.S. At short ranges, the structure is effectively a layer over a half space. At greater ranges, the structure appears to have a smooth positive gradient.

or nonexistent gradient and the study of Helmberger (1973) shows that it is underlain by a substantial low velocity zone. The LVZ extends downward to about 175 km where the P velocity finally once more exceeds that of the lid.

In a structure such as the one in Figure 4, the strong discontinuity at the base of the crust forms an efficient energy trap. The weak lid gradient and low velocity zone cause an effective shadow zone. The Helmberger and Engen (1980) procedure for modeling the trapped energy entails summing all possible generalized rays in the layer over a half space which arrive within the time window of interest. This typically involves as many as 4094 separate generalized rays for a time window of 90s. In the Burdick and Helmberger (1978) approach to modeling energy from the mantle, only one generalized ray (the direct reflection is computed from each velocity layer from the lid downward. Burdick and Orcutt (1979) have shown that this is an acceptably accurate approximation. The relative contributions at regional ranges of energy trapped in the crust versus energy turning in the mantle are shown in Figures 5 and 6. Figures 5a to 5c show Green's functions computed from just the generalized rays trapped in the crust. Solutions are shown for the three fundamental double couple fault types with an assumed source depth of 8 km in the crust layer. The long period precursor is made up of various head waves beginning with  $P_n$ . The sequence of high frequency crustal resonance phases initiates with the PmP energy. In a generalized ray context, these would be thought of as head wave and reflected contributions from the same generalized ray. Comparable Green's functions are shown in Figures 6a to c with the addition of the primary rays from the upper mantle. They exhibit modest high frequency arrivals near the front of the Green's functions beginning at about

# VERTICAL STRIKE SLIP GREEN'S FUNCTIONS

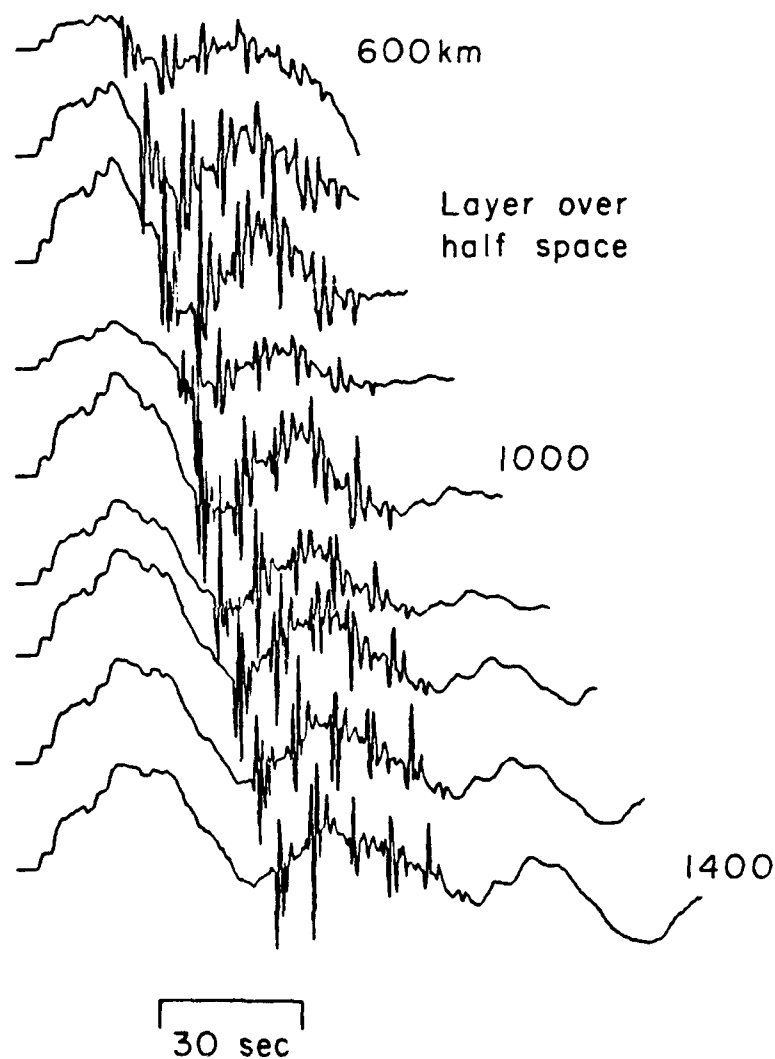


Figure 5a. Green's functions for a layer over a half space computed using the methodology of Helmberger and Engen (1980).

VERTICAL DIP SLIP  
GREEN'S FUNCTIONS

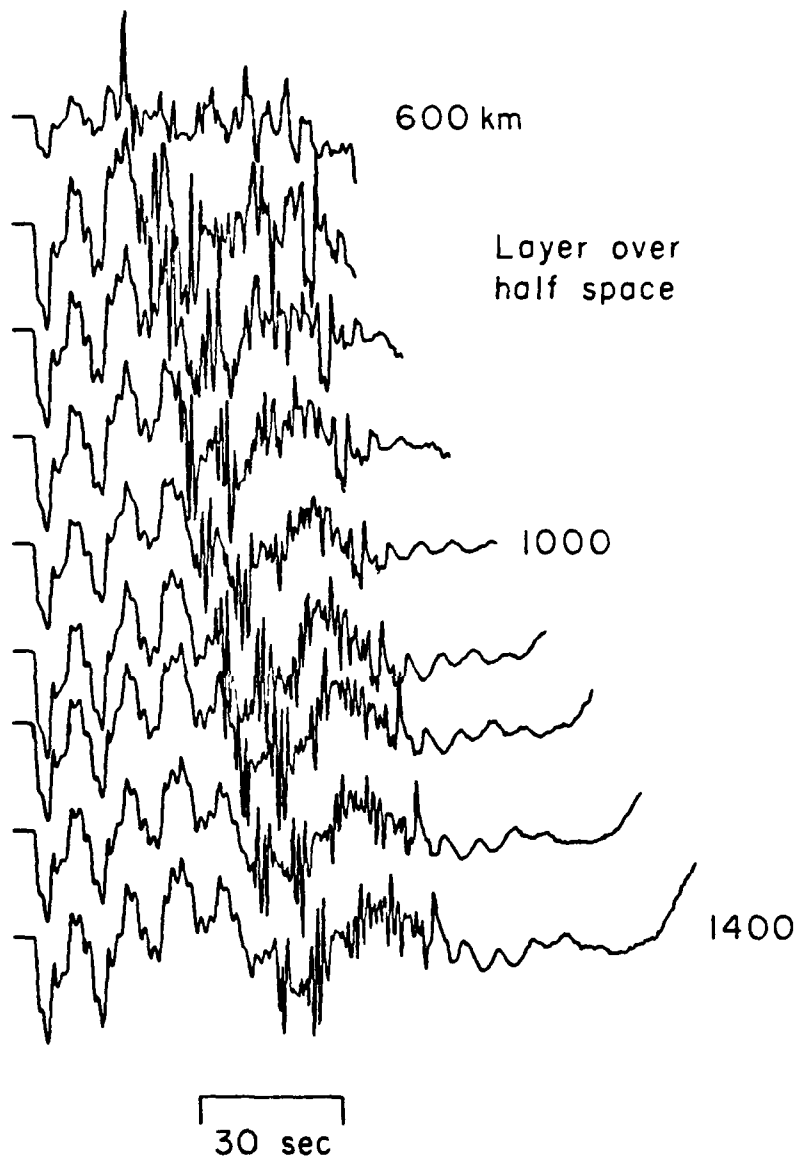


Figure 5b.

45° DIP SLIP  
GREEN'S FUNCTIONS

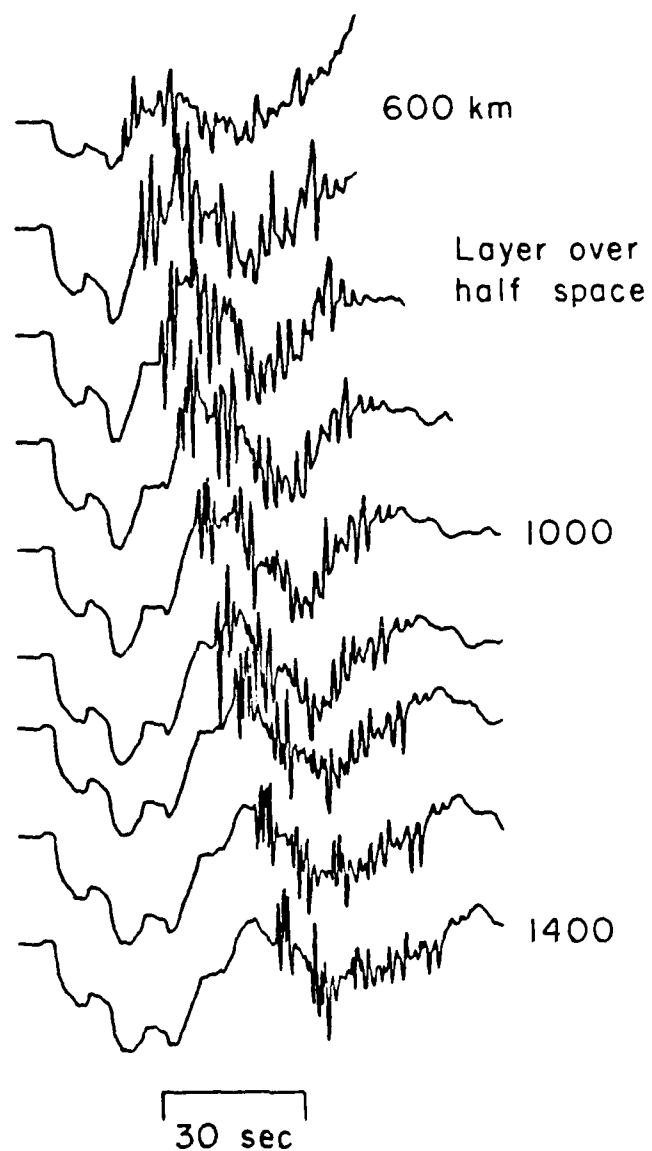


Figure 5c.

# VERTICAL STRIKE SLIP GREEN'S FUNCTIONS

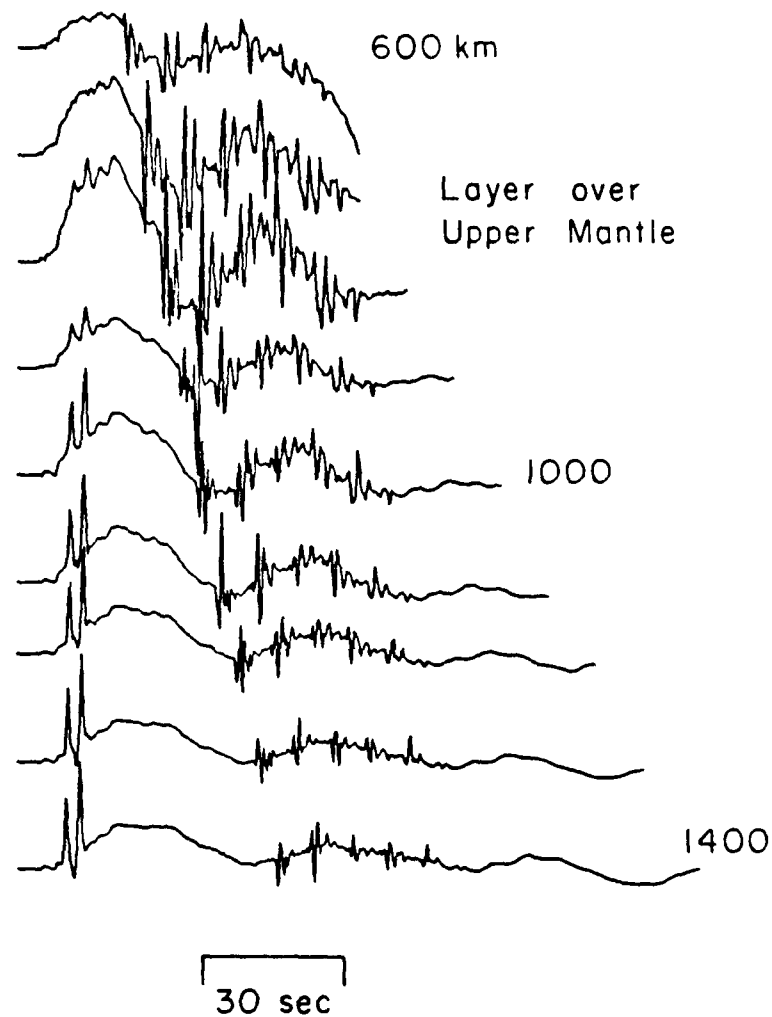


Figure 6a. Green's functions for the model shown in Figure 4. The ray sets specified by Helmberger and Engen (1980) were computed for the top layer while only the primaries were computed for deeper layers.

VERTICAL DIP SLIP  
GREEN'S FUNCTIONS

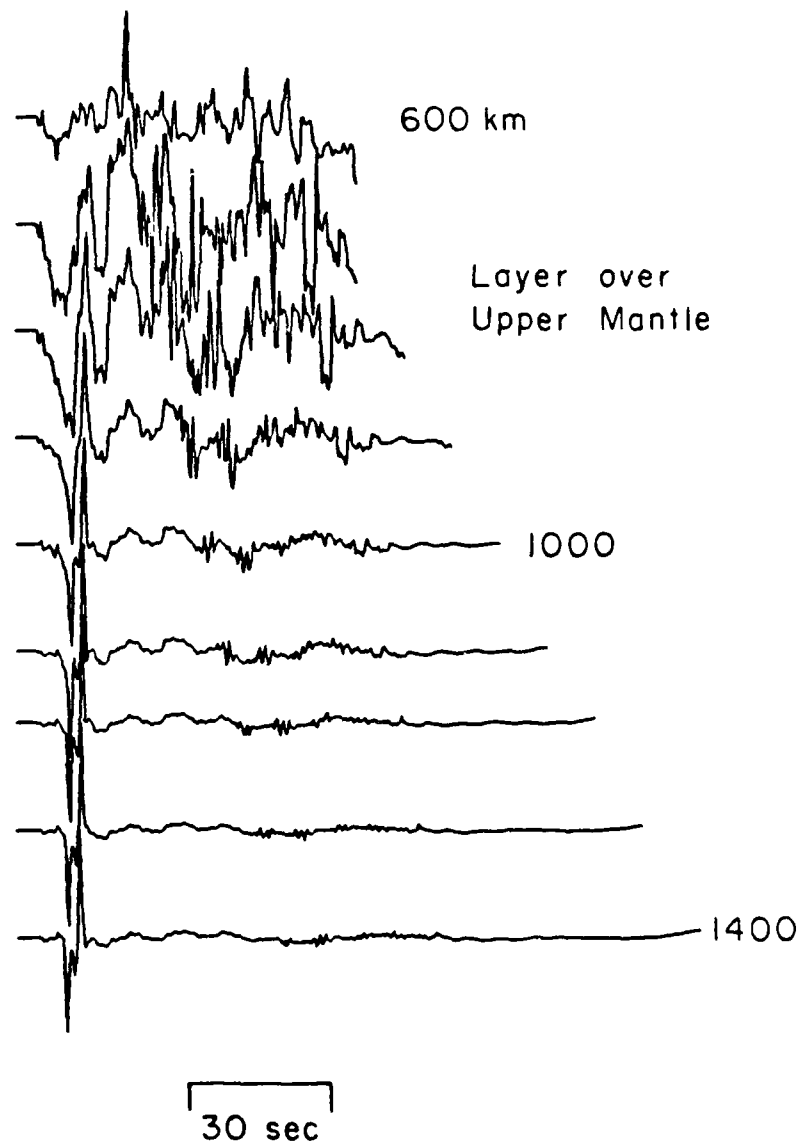


Figure 6b.

45° DIP SLIP  
GREEN'S FUNCTIONS

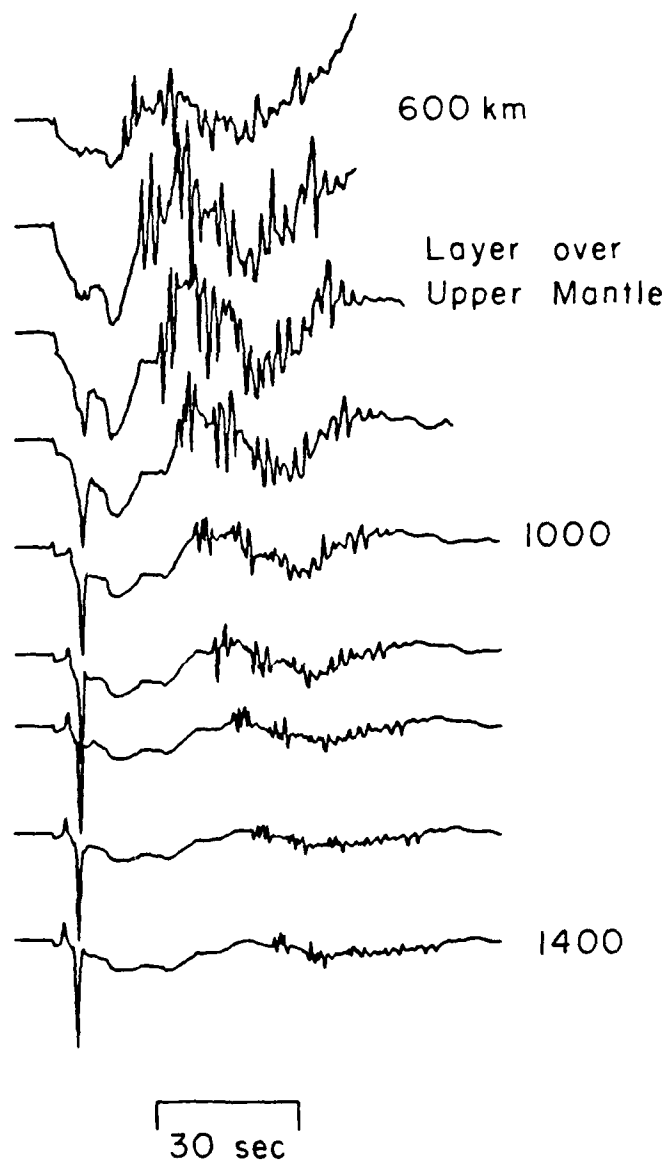


Figure 6c.



1000 km, but this energy does not become highly significant until about 1200 km. The crustal resonance phase section of the time series remains similar at all ranges shown in Figures 5 and 6.

A simple layer over a half space is a highly simplified model. Nonetheless because of the weak lid gradient and the low velocity zone in the western U.S., such a model can be used to produce accurate synthetics. Figure 7 shows a profile of observed records at WWSSN stations from two western U.S. events that clearly exhibits the wave propagation effects predicted in Figure 6. At close ranges, the signals have an emergent, long period onset followed by a large  $P_L$  oscillation. At ranges beyond 1200 km, the arrivals have a sharp, high frequency beginning and the  $P_L$  energy moves substantially back in the trace. In the following sections, we will discuss the development of crustal resonance phases in a layer over a half space and illustrate why they have a high potential for aiding in discrimination decisions.

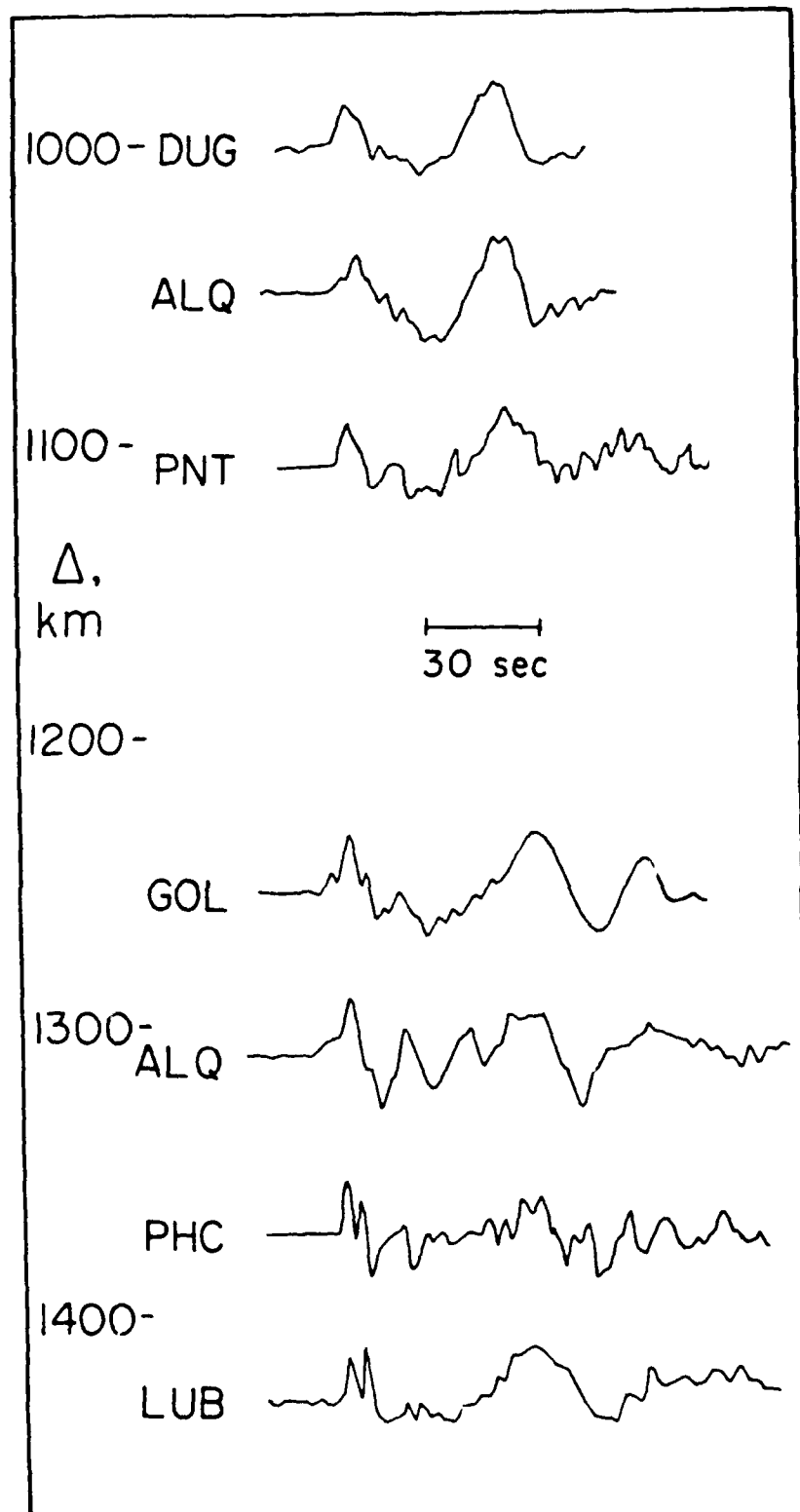


Figure 7. Typical records from two strike slip earthquakes (El Golfo and Truckee) in the western U.S. Displayed as a function of range. The first energy is emergent at closer ranges since it is long period  $P_n$ . It is sharper at greater ranges since it eventually becomes a turning ray in the upper mantle.

## CRUSTAL RESONANCE PHASES

A generalized ray representation of the response of a crust model is particularly well suited for determining exactly how prominent arrivals such as crustal resonance phases are being excited. The Green's function can be built progressively by adding in more rays until the feature of interest emerges. Figure 8 shows the response of the Helmberger and Engen (1980) crust model at a distance of 1000 km being constructed through sequential ray addition.

Two of the four fundamental Green's functions are shown; vertical strike slip on the left and vertical dip slip on the right. These two fundamental Green's functions produce the most variable  $P_{n1}$  waves because they have the strongest variation in vertical radiation pattern as shown at the top. Results from this figure apply equally as well to the other two fundamental Green's functions. The response due to just the direct P and S rays is shown first. Then we show the effect of adding in all rays with just one reverberation in the crust along with associated depth phases (PmP, pPmP, SmP, sSmP etc.). The third response is for two reverberations in the crust with depth phases, the fourth for four and so on. The number of additional rays in each iteration is indicated. The number of rays grows so rapidly with each iteration that considering any more than 5 reverberations would be impractical. Fortunately, it appears that the long period onset of the Green's function stops evolving after three reverberations are added in. About the first 20 seconds of the high frequency  $P_g$  seems to have stabilized also, and this is all that is necessary for the purposes of this study. The crustal resonance phases appear most clearly in the strike slip Green's

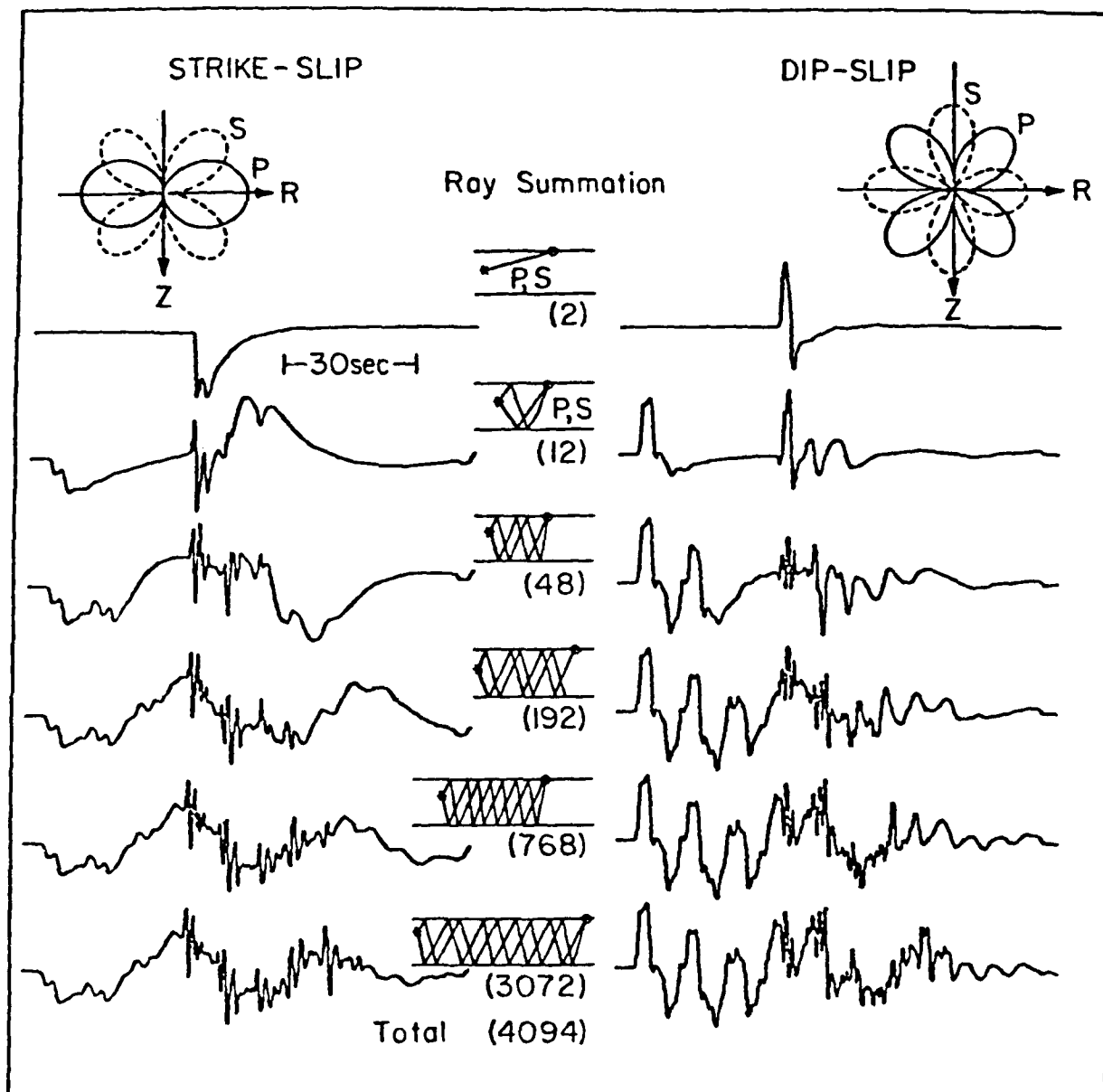


Figure 8. Green's functions computed using the methodology of Helmberger and Engen (1980). Successive rows are computed by adding in more crustal reverberations as indicated. The strike slip and dip slip results vary substantially because of the difference in vertical radiation pattern.

functions on the left. It is clear from the way that the early resonances appear after just a few rays are added in and do not change, while later resonance phases appear only when additional reverberations are considered, that the rhythmic pattern of resonance phases is caused by complicated interferences of rays with successive numbers of bounces in the crust.

We shall examine the composition of the first two resonance phases in more detail. Still referring to Figure 8, we note in the top trace that the direct rays contribute a long period arrival at the time of the first crustal resonance which appears to be composed of two pulses. Further analysis shows that these two pulses are direct P and the SP head wave along the free surface. The resonance phase almost develops completely after the first order reverberations are included and stabilizes entirely after two. In Figure 9, we compare the four fundamental Green's functions generated from all 254 rays in the first three crustal reverberations to responses generated from those 6 rays which contribute most strongly to the first crustal resonance phase. These rays are listed in Table 1. As expected, they include PmP, SmS and their unconverted depth phases pPmP and sSmS along with the direct waves. As shown in Figure 8, the direct phases cause a long period pulse. The high frequency character of the first crustal resonance phase is controlled by the strong interference of PmP and SmS with their depth phases.

The two most important source characteristics on which an effective discriminant might be based are event radiation pattern and event depth. The possibilities for basing a radiation pattern discriminant on the first resonance phases may be assessed by comparing the explosion arrival to the three fundamental double couple arrivals. An arbitrary double couple Green's

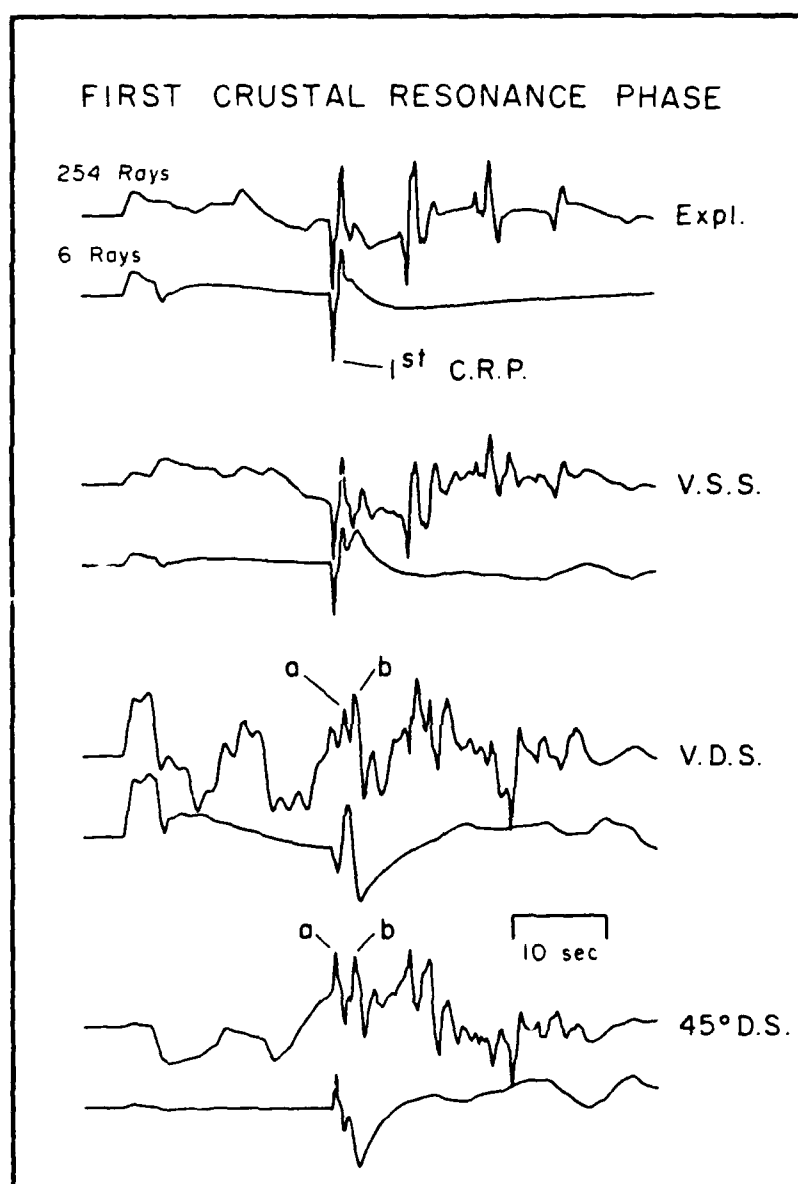


Figure 9. Analysis of the composition of the first crustal resonance phase. The lower traces which contain most of the energy in the first C.R.P. were computed with only the 6 rays listed in Table 1. The upper traces were computed from a much more complete ray set.

<p> <b>           RAYS IN THE FIRST            CRUSTAL RESONANCE PHASE         </b> </p>	<p> <b>           RAYS IN THE SECOND            CRUSTAL RESONANCE PHASE         </b> </p>
<p>           P            S            PmP            pPmp            SmS            sSmS         </p>	<p>           PmS            SmP            pSmS            sPmP            PmPSmS            SmSPmP            PmPSmP            PmSPmP         </p>

Table 1.

function could be represented as a weighted sum of the the fundamental three. A strike slip earthquake would clearly be the most difficult to distinguish from an explosion based on radiation pattern. The vertical dip slip resonance phase is longer in period and is interfered with more strongly by other phases. The actual first resonance phase pulse is labeled "a". We shall discuss the origin of the second peak labeled "b" when investigating the composition of the second resonance phase. The 45° dip slip event Green's function has a reversal in polarity with respect to the explosion and also exhibits the "a" and "b" peaks. It would thus seem that a measure of the first crustal resonance phase complexity could turn out to be a reasonable radiation pattern discriminant for separating dip slip earthquakes from explosions and strike slip earthquakes. Other discriminants would be needed for further separation of the latter two types of events. The layer over a half space model does not predict any substantial variation of the Green's functions with the range of source depths between explosions and earthquakes. However, in the real earth there are strong gradients near the top of the earth which amplify depth effects. The properties of the first crustal resonance phase may thus still provide some strong depth discriminant potential. We will discuss this possibility in a later section.

The rays important to the second crustal resonance phase are given in Table 1 and the response from just these rays is compared to the complete Green's function in Figure 10. Interestingly, the second resonance phase is not dominated by rays with a complete extra reverberation in the crust but by those which have at least one converted leg. It appears that a radiation pattern discriminant based on the second crustal resonance phase would again be most effective in separating just dip slip events from explosions and



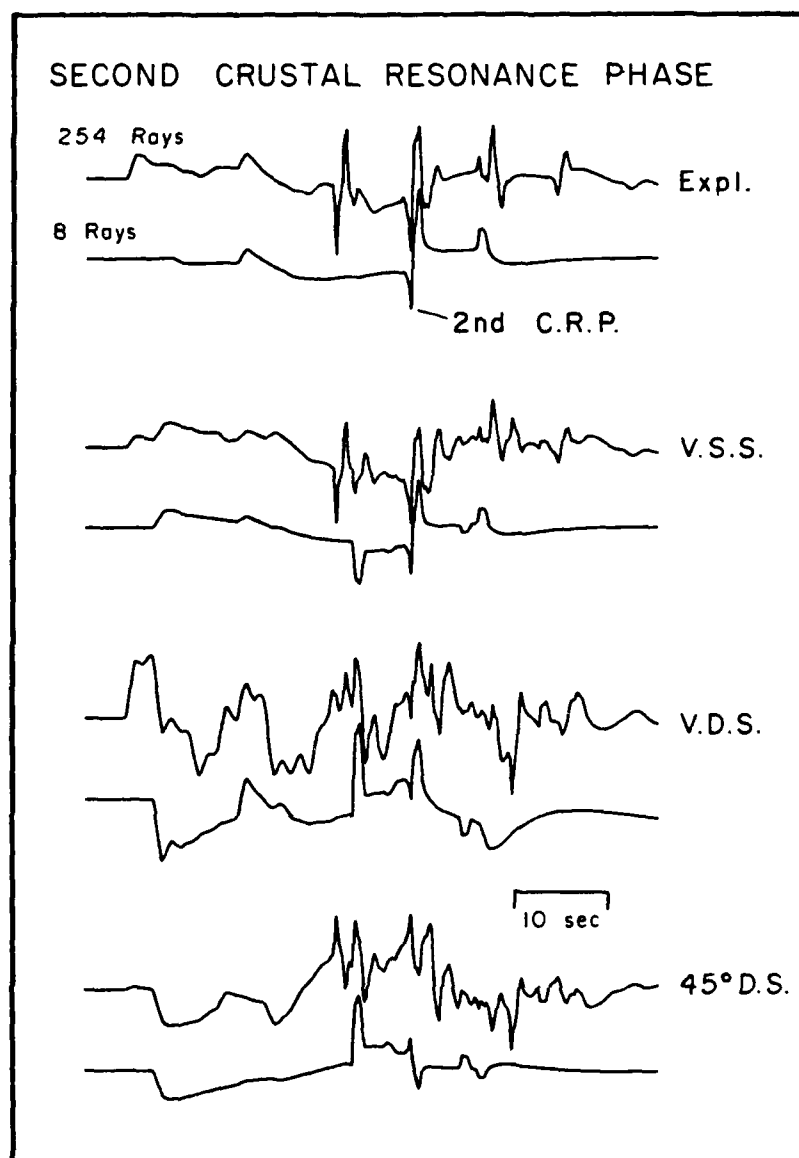


Figure 10. Analysis of the composition of the second crustal resonance phase. The lower traces which contain most of the energy in the second C.R.P. were computed using only the 8 converted rays listed in Table 1. The upper traces were computed from a much more complete ray set.

strike slip events. The arrival labeled "b" in Figures 9 and 10 turns out to be a converted phase and therefore more appropriately grouped with the second crustal resonance. It is, however, caused by sPmP and therefore arrives close to PmP for shallow sources. Again, depth effects are strongly under predicted by a layer over a half space crust model, so it is difficult to determine whether the second resonance phase has discrimination potential based on source depth.

## OBSERVATIONS AND MODELS OF CRUSTAL RESONANCE PHASES

In the preceding, we have shown that crustal resonance phases have a high potential for enhancing discrimination capabilities. In this section, we demonstrate that they are stable enough at intermediate to long periods (perhaps 2 to 50s) so that they can be reliably predicted. This implies that it would be very reasonable to predict a synthetic  $P_{n1}$  record for an event too small to produce any long periods itself and that this synthetic could be reliably used to aid in the analysis of the observed signal. The data sets we will consider contain WSSN records from several different NTS explosions and from a moderate sized earthquake which occurred very near to the test site. We begin with the explosion.

Figure 11 displays the  $P_{n1}$  observations from NTS as a seismic section. The closest observation is from DUG at a range of 453 km and the most distant is from LUB at a range of 1386 km. All but the first trace are the vertical component, but both data and synthetic  $P_{n1}$ 's exhibit only slight differences between the radial and vertical motions. It was necessary to compile the data set from several different source events since no one event was recorded well at every station. The vertical line is the estimated first arrival time and the other line shows the predicted move out of PmP for the Helmberger and Engen (1980) layer over a half space crustal model. The abrupt change of frequency content signaling the arrival of  $P_g$  at the PmP arrival time is apparent in all traces except LON. The  $P_n$  appears initially as a very long period phase but then becomes much sharper at ranges past 1000 km just as did the signals in Figure 7. The first arrival at these larger ranges is penetrating the low velocity zone and turning against the positive gradient in

# NTS EVENT $P_n$ RECORDS

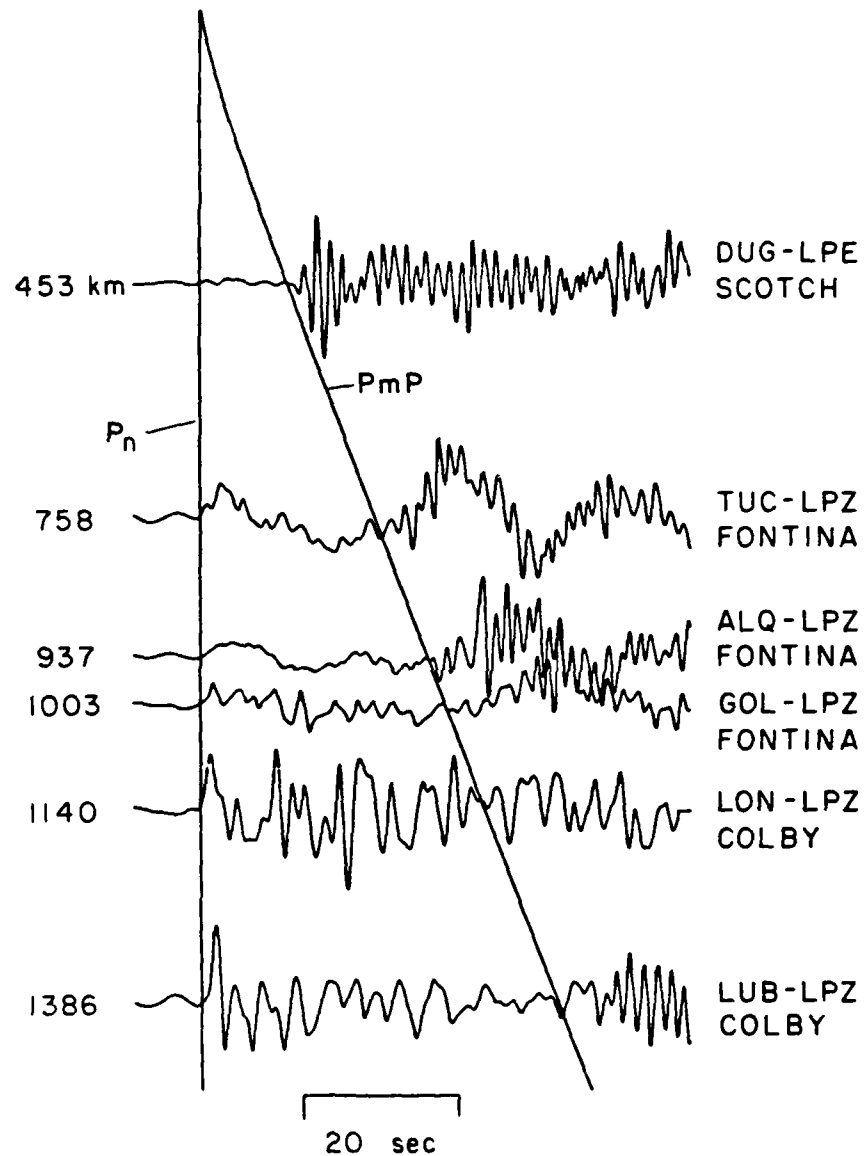


Figure 11. Long period WWSSN records of NTS blasts at regional ranges displayed as a seismic section.

the upper mantle. As it does so, it begins travelling faster than  $P_n$  so that at the greatest ranges the separation between the first arrival and  $P_g$  is no longer predicted by the layer over a half space model.

It is necessary to equalize the explosion records to a common source time history since we are not interested in effects associated with variations of this sort. To do so we use the procedure outlined by Murphy (197), however we use the alternate source time function and scaling laws given in Burger et al. (1987). We chose to correct the events all to a common size of 1000 kt. The yields for unannounced events were estimated using the magnitudes and magnitude yield relation given in Burger et al. (1988). The source equalized records are shown in Figure 12. A comparison between Figures 11 and 12 demonstrates that the effects of variation in yield are not strong. As a final step in the processing of this seismic section, we wish to equalize the records for direct comparison with those from the earthquake. As we discuss in the following, a good representation of the source of the earthquake is a trapezoid with rise and fall times of .4s and a level time of .5s. In Figure 13, we show the explosion record section with this source function convolved through. To directly equalize the records to the earthquake records, we would need to deconvolve the explosion source. Unfortunately, this is a numerically unstable process which apparently introduces spurious features. As an alternative, we will cross convolve the sources; that is we shall convolve the explosion records with the theoretical earthquake source and the earthquake records with the theoretical explosion source. That way all records will approximately contain the effects of both sources. A comparison of Figures 11, 12 and 13 shows that all of these source corrections have very little impact.

SOURCE EQUALIZED (1000 kt)  
NTS EVENT  $P_n$  RECORDS

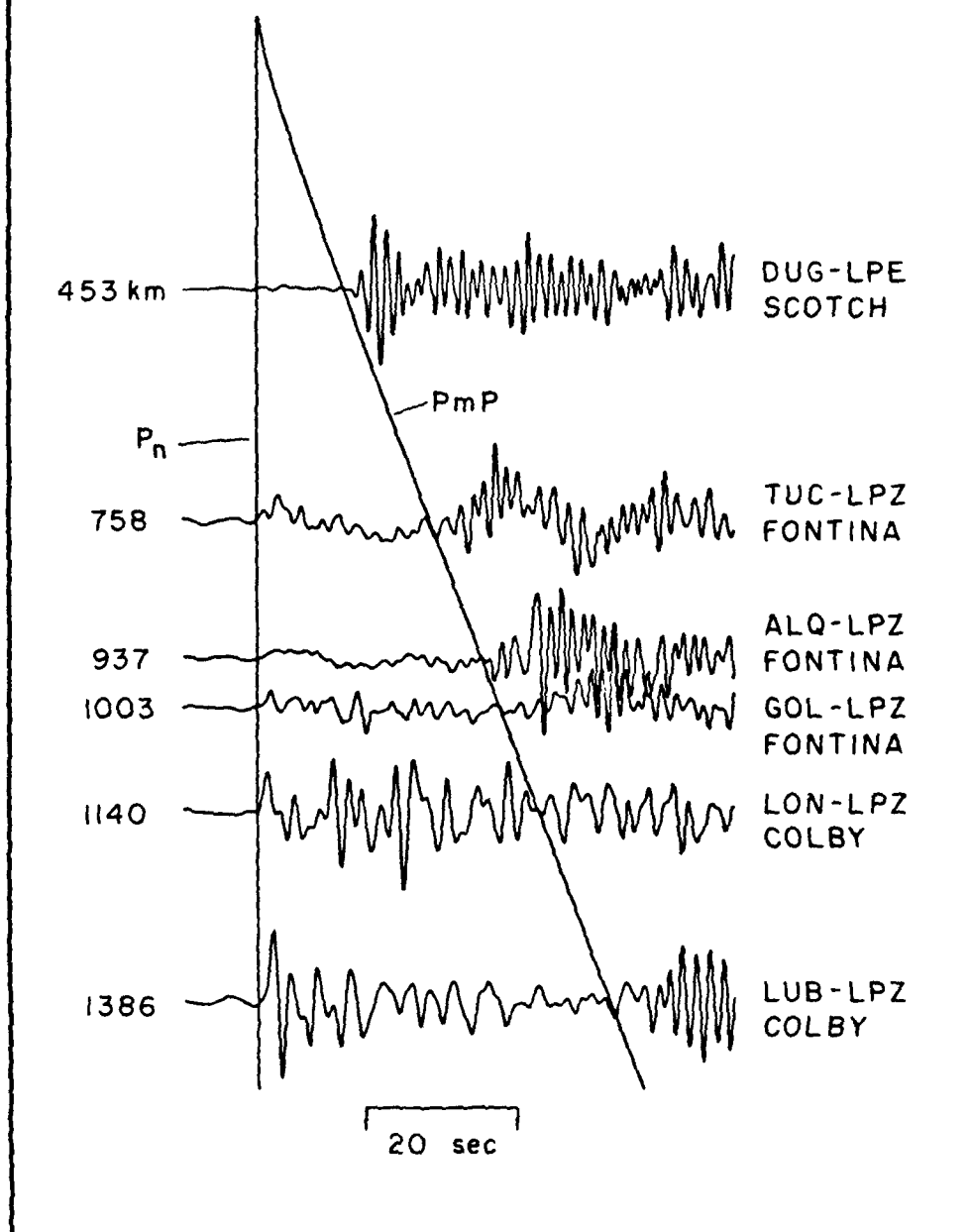


Figure 12. The NTS regional seismic section corrected to a common explosion source time history.

# CROSS CONVOLVED NTS EVENT $P_n$ RECORDS

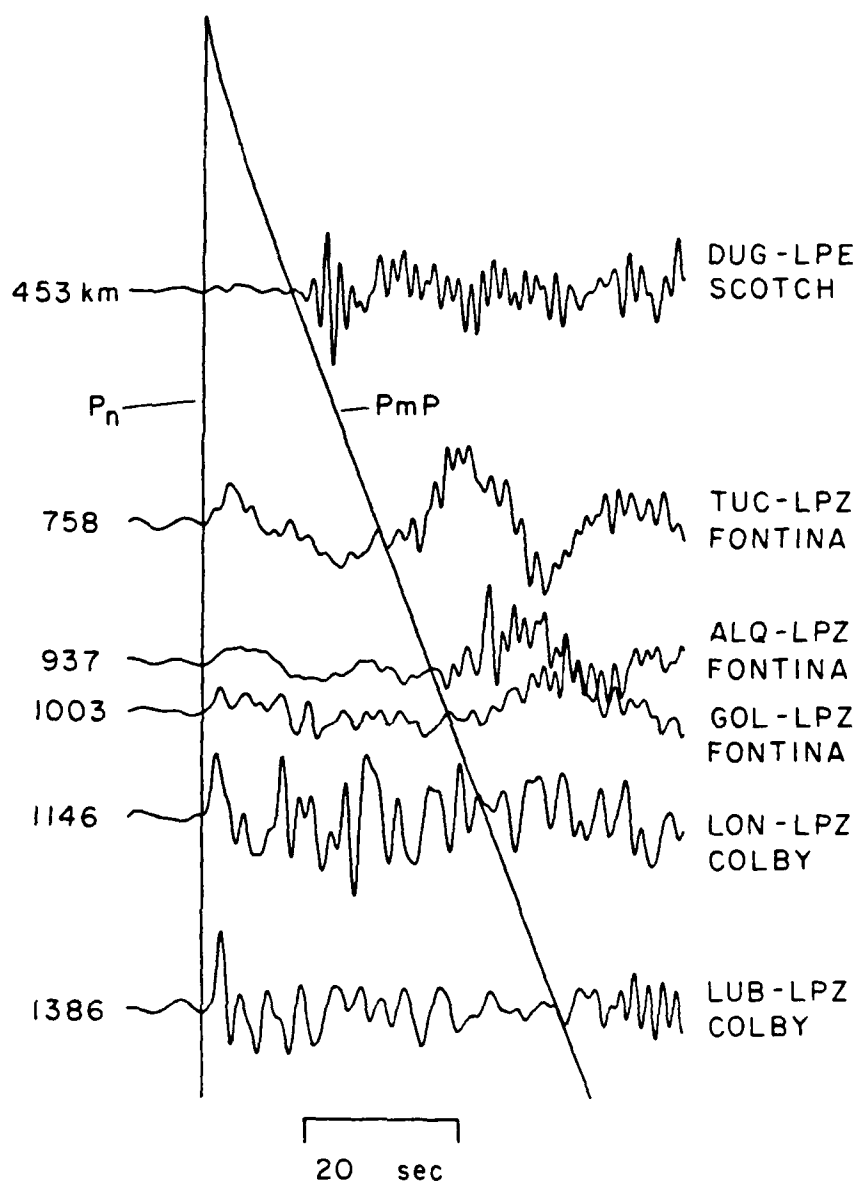


Figure 13. The NTS regional seismic section convolved with the theoretical source time function for the Caliente earthquake.

The earthquake records we shall analyze are from the 8/16/66 Caliente earthquake ( $m_b = 5.6$ ). It was previously studied by Wallace et al. (1983) who provided a focal mechanism and source time history for it. It is their trapezoidal time history which was used above to generate the cross convolved section of explosion observations. The event was shallow with a strike slip mechanism and was located about 150 km east of the northeast corner of NTS. The  $P_{n1}$  records from the event are displayed in a seismic section directly comparable to the explosion section in Figure 14. The long period  $P_n$  train moving ahead of the  $P_g$  is very clear once again. It is of some interest to compare the LUB records in the two sections. In the Caliente section, the station is closer to the source by 191 km, so the first arrival remains emergent. The first arrival to PmP lines correctly predict the onset of  $P_g$  and the  $P_g$  energy is much larger than the  $P_n$ . None of these factors are the same at the greater distance for the explosion because the first energy has begun to speed up and turn against a positive mantle gradient. It should be noted that in both of these sections the record at GOL comes from a longer period instrument (30-90 vs 15-100). To equalize the records to the explosion records we convolve in an estimate of the explosion source. The resulting traces, shown in Figure 15, are just slightly smoothed from the original. The differences in the records in the cross convolved sections in Figures 13 and 15 should reflect primarily the differences in radiation pattern and in source depth. This is the type of information on which it is most likely that we will be able to base more effective types of discriminants. The most striking difference is that even after source equalization the explosion resonance phases appear to be higher in frequency content. This is the type of effect



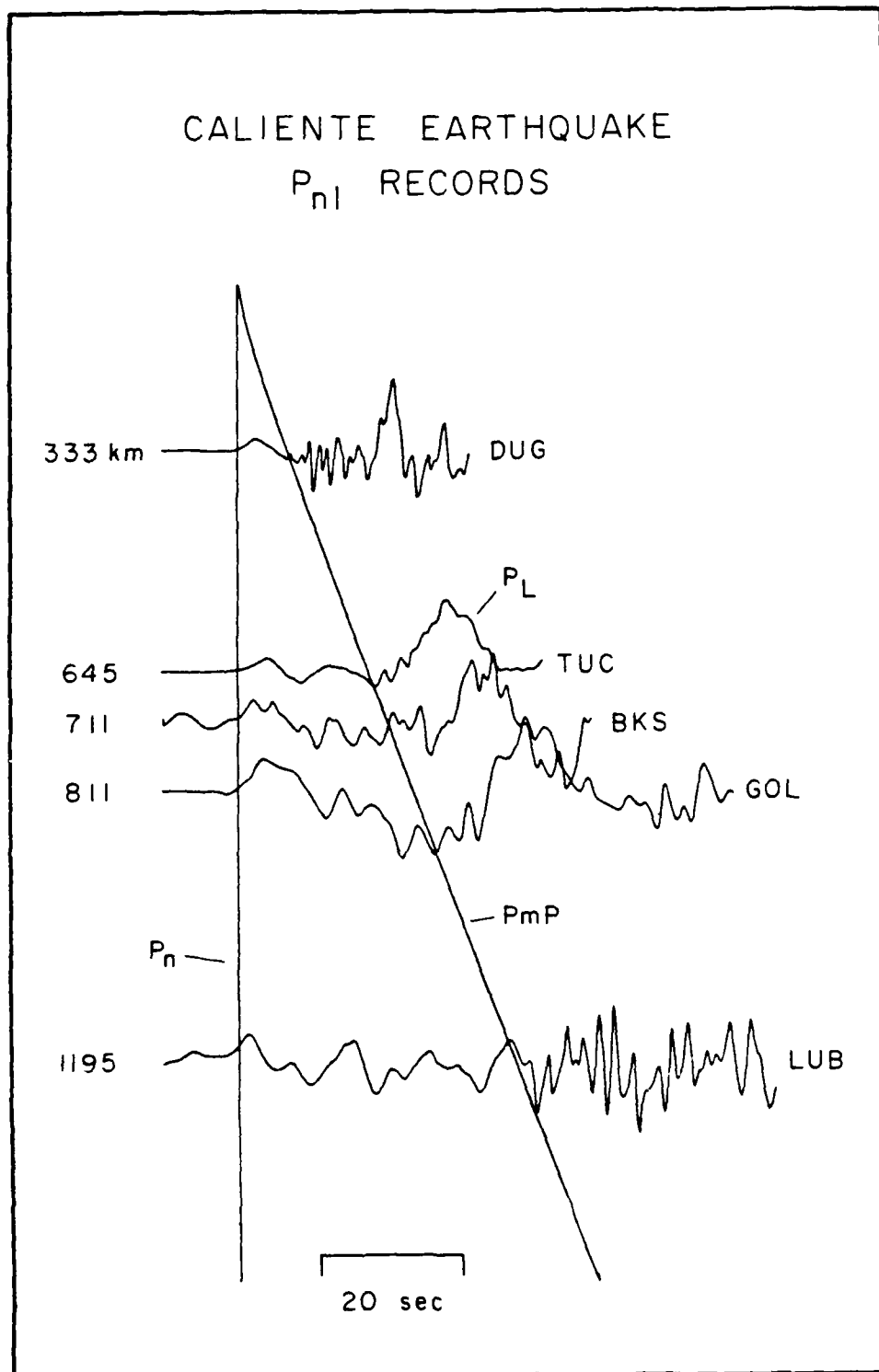


Figure 14. Long period WWSSN records of the Caliente earthquake at regional ranges displayed as a seismic section.

# CROSS CONVOLVED CALIENTE EARTHQUAKE $P_{nl}$ RECORDS

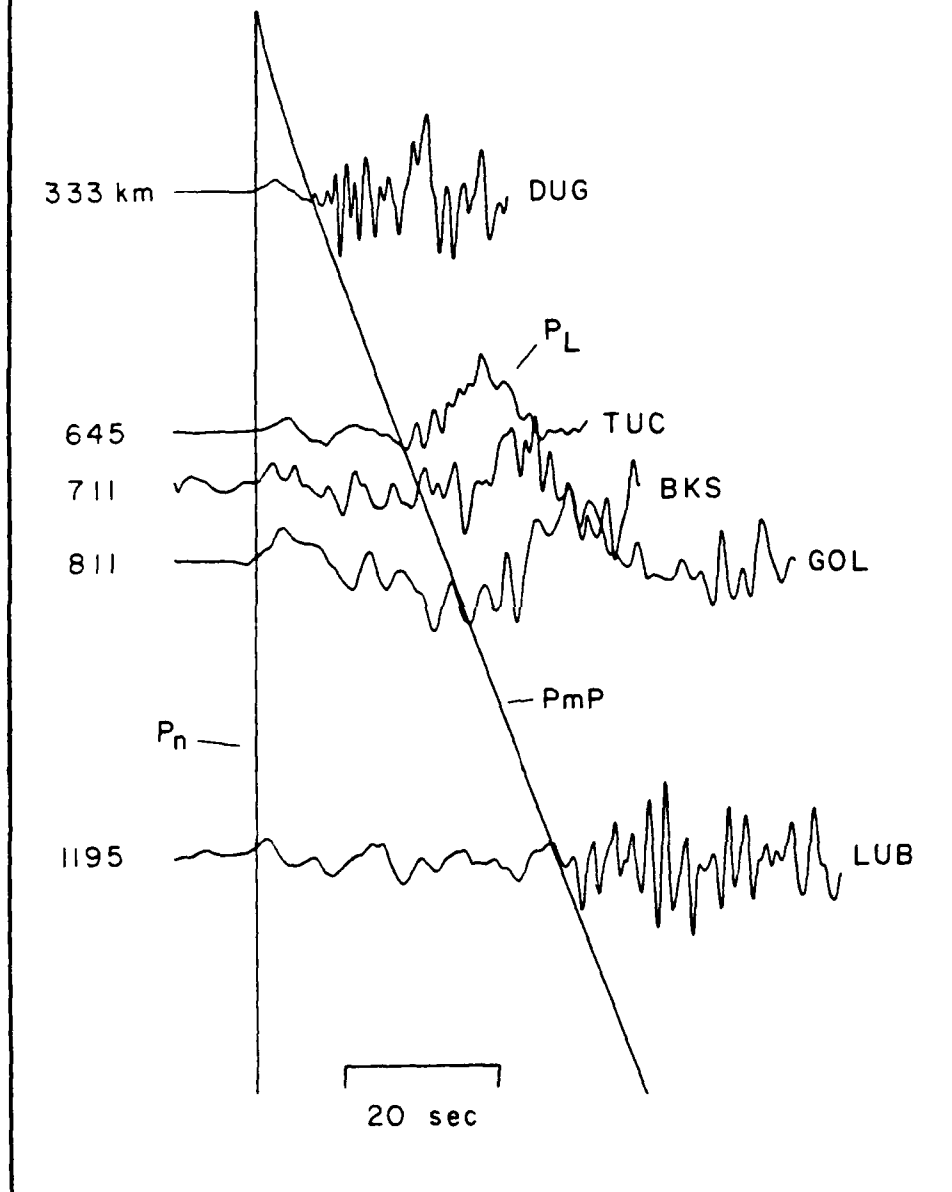


Figure 15. The Caliente regional seismic section convolved with the theoretical source time function for a 1000 kt nuclear event.

one might expect to occur due to the significant differences in source depth. The cause of this shift in frequency can be explored through synthetic seismogram modeling.

We begin with a discussion of the earthquake records because they are easier to explain. The synthetics are computed by assuming the source mechanism and time function of Wallace et al. (1983) and computing Green's functions following the methods of Helmberger and Engen (1980). A frequency independent  $t^*$  of 0.25s is assumed for all rays since no more sophisticated assumption is warranted. A comparison between the data and synthetics for 7 different stations is shown in Figures 16a through g. The traces are shown on a large scale because we wish to show that some of the fine details in the data and synthetics associated with the arrival of the crustal resonance phases correlate very well.

The closest station, DUG, is shown first. The Green's function is shown at the top, the observed trace in the center and the synthetic at the bottom. The first vertical line signifies the first arrival and the second shows the time for PmP predicted by the layer over a half space crust model. The observed record at DUG is perhaps the most poorly fit of the earthquake records because it contains more high frequency than is predicted by the synthetic. In this case, we only argue that the synthetic correctly predicts the onset of  $P_g$  and that this is the time of arrival of the first crustal resonance. The synthetic also predicts the long period character of the data. In cases like this, it should be a least possible to compute synthetics, use them as a guide to identify times at which important information is arriving in the signal (i.e. depth phases) and to try to build a discriminant from this

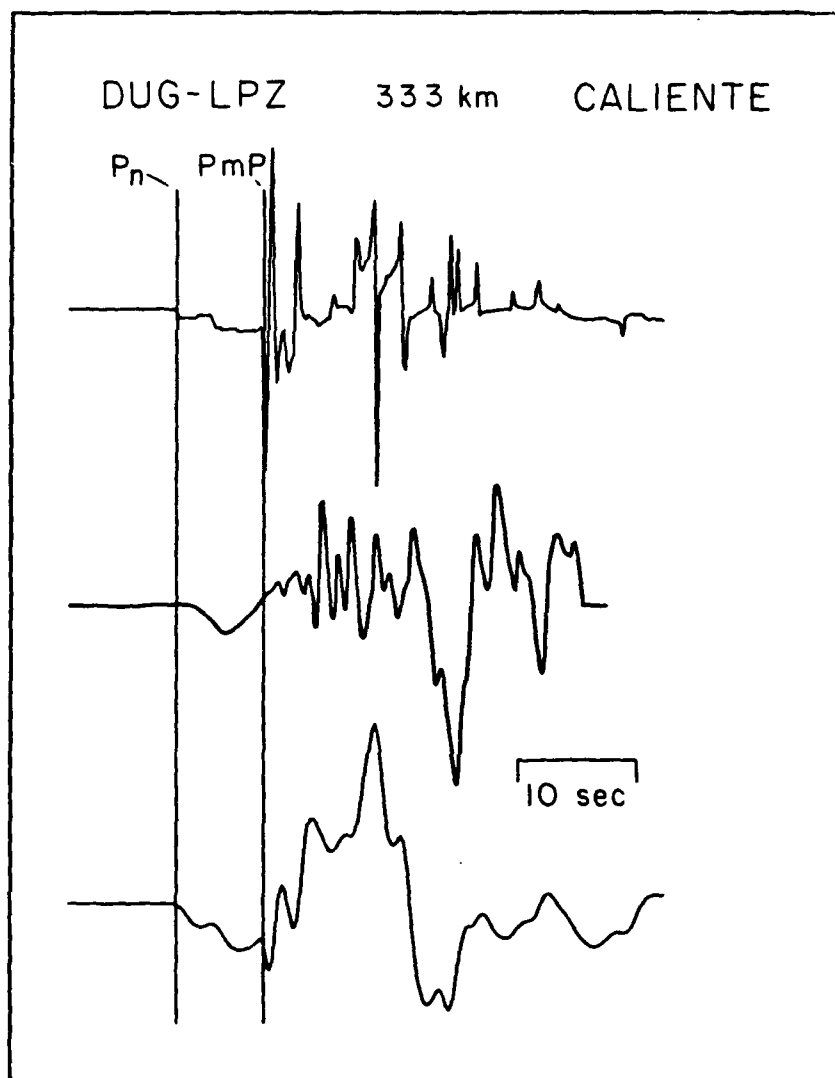


Figure 16a. A comparison between observed and synthetic  $P_{n1}$  records of the Caliente earthquake. The Green's function is shown at the top, the data in the center and the synthetic at the bottom. The vertical lines show the arrival of  $P_n$  and  $PmP$ .

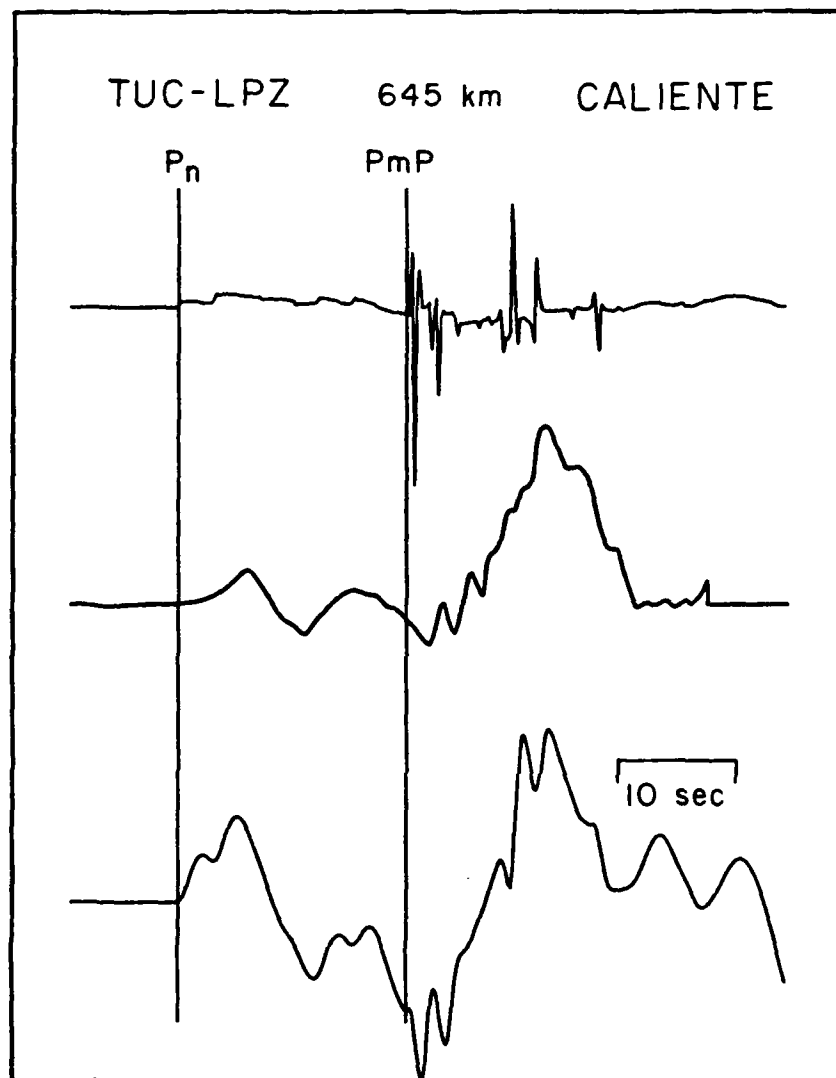


Figure 16b.

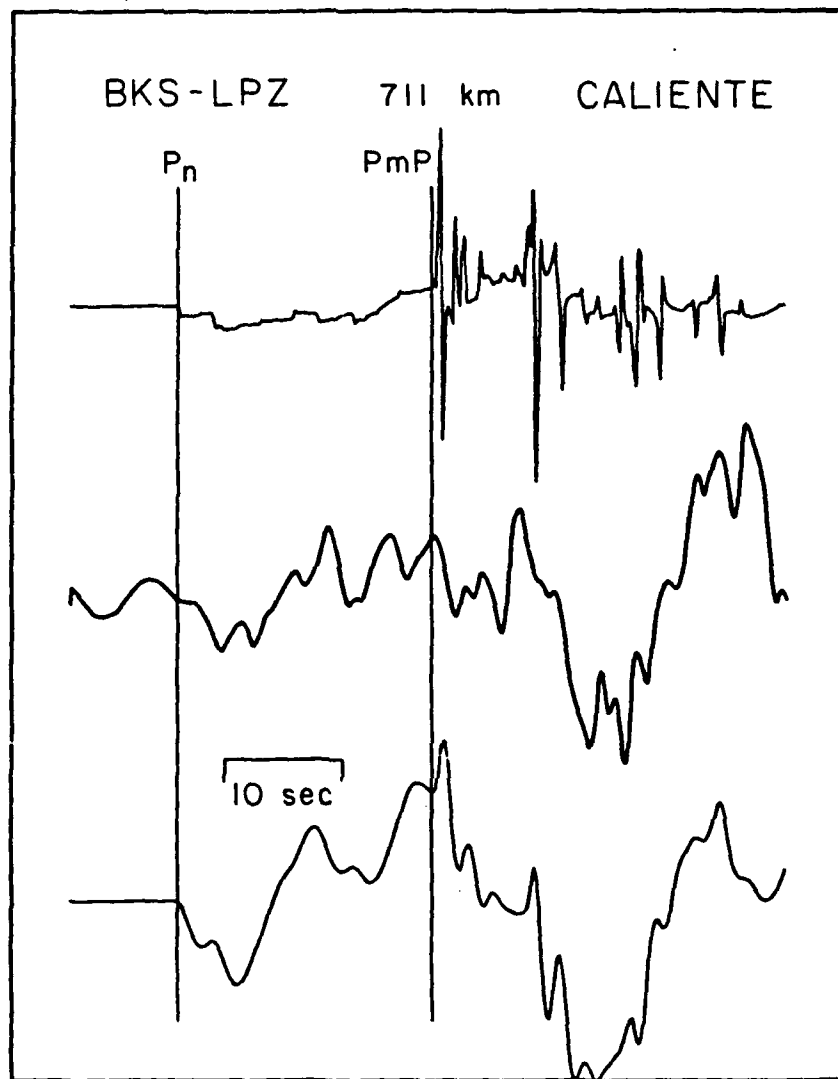


Figure 16c.

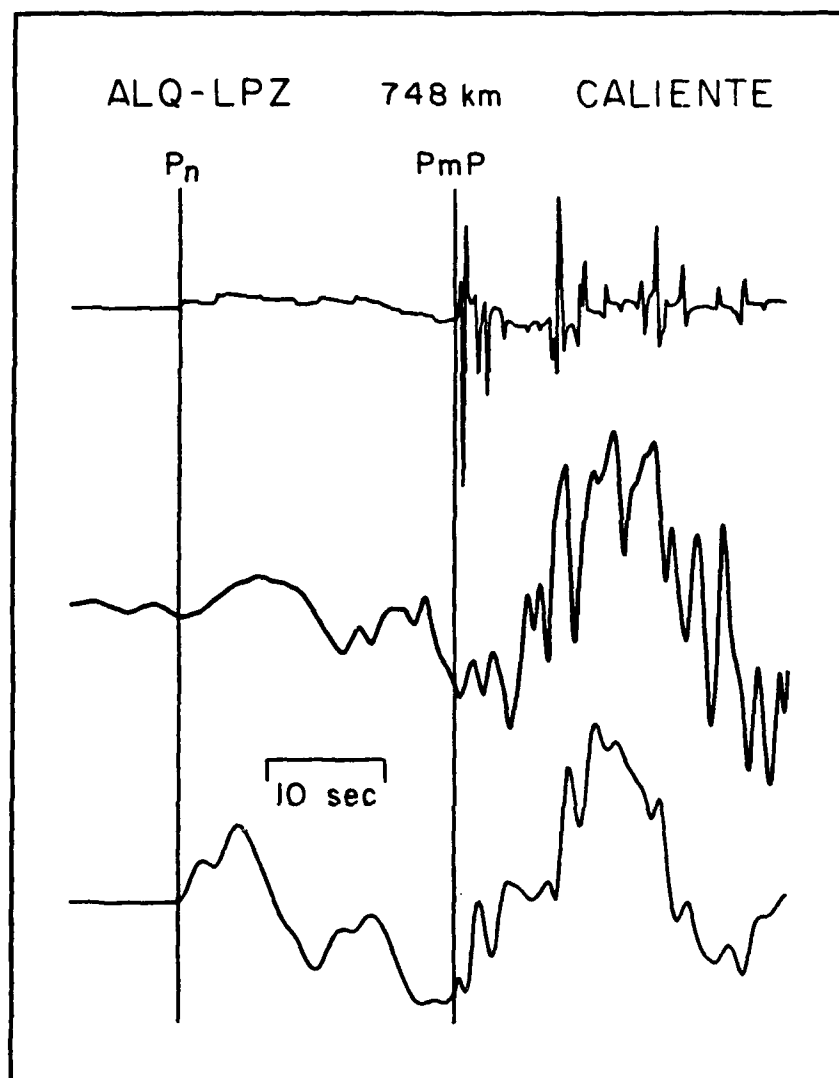


Figure 16d.

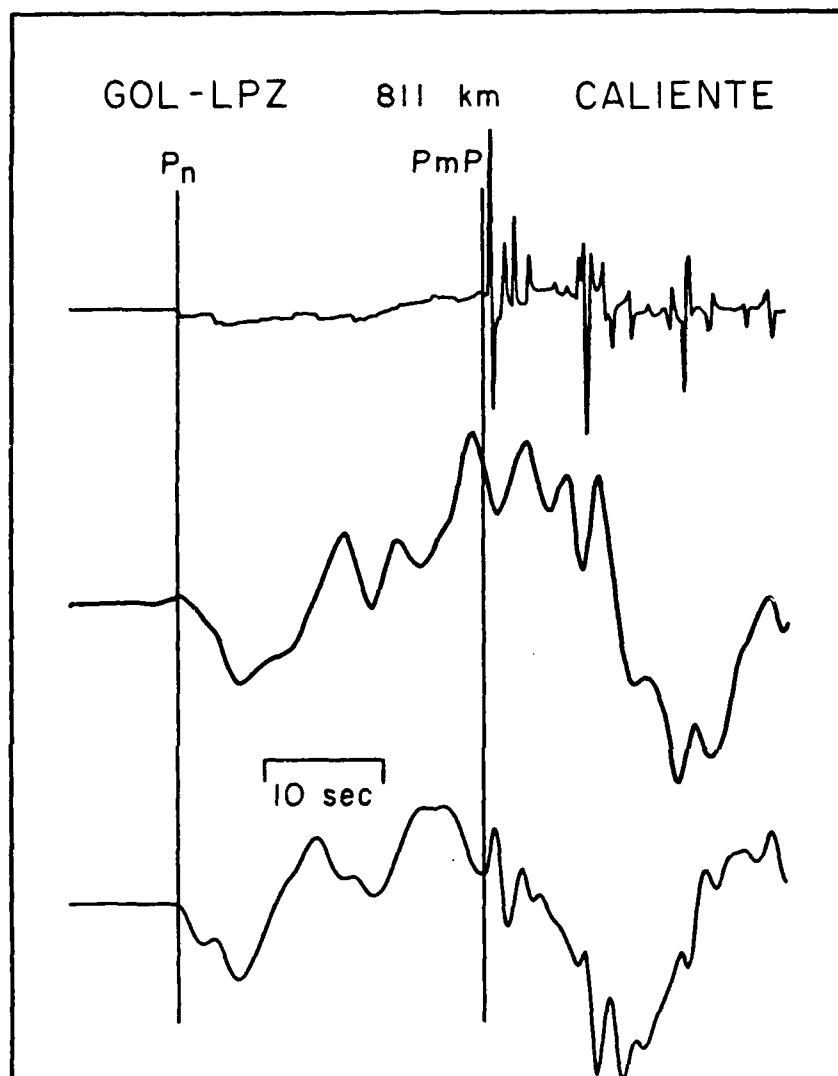


Figure 16e.



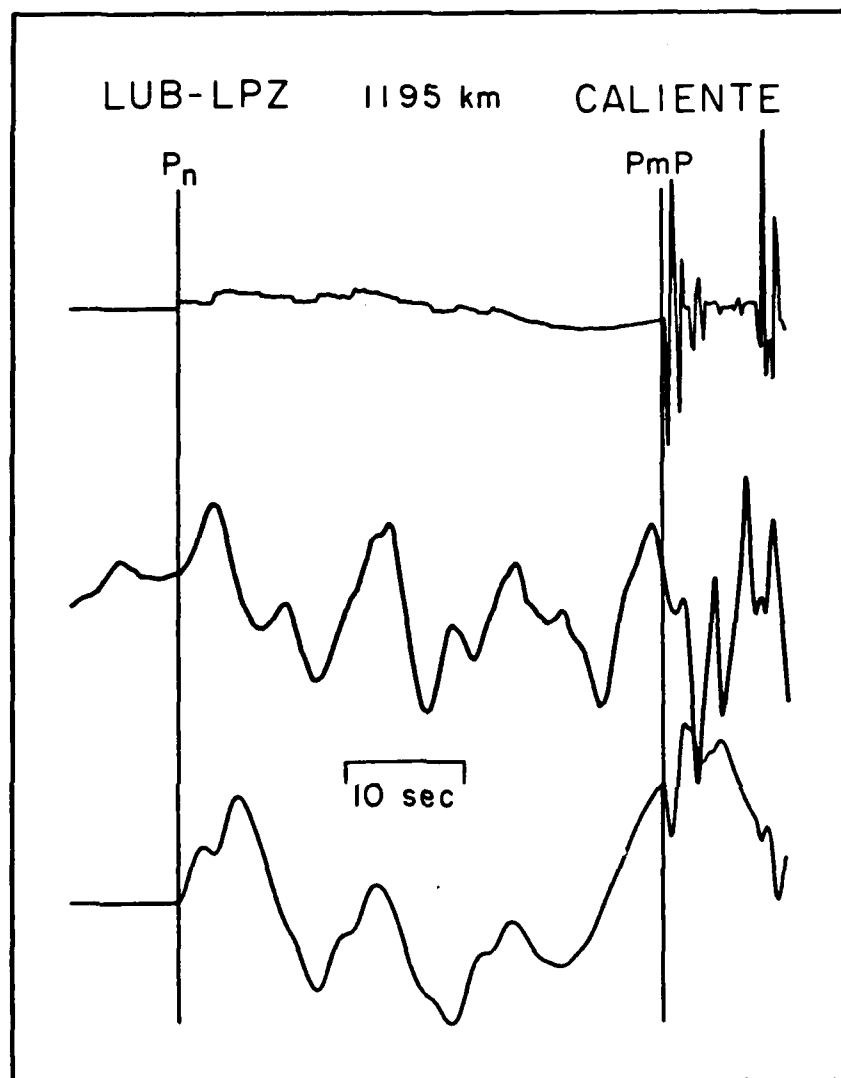


Figure 16f.

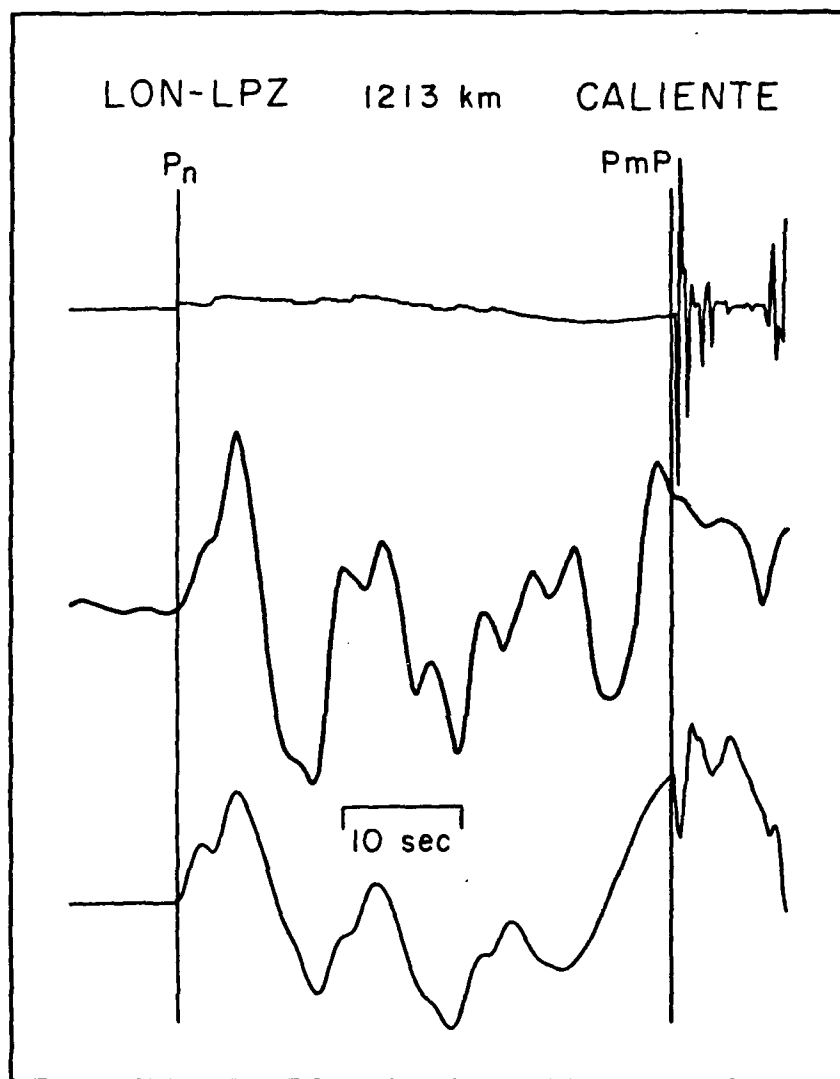


Figure 16g.

information semi-empirically.

The second record at TUC is fit much more closely. The match of the double-peaked structure at the arrival time of the first crustal resonance is quite remarkable. Features specifically associated with the arrival of the second crustal resonance are also apparent. The close match demonstrates that we can deterministically predict in records from the western U.S. the arrival time of depth phase information and converted phase information. The short period records from small events could be scrutinized in these time windows in order to discriminate those that are probably explosions. It is also important to note that the general frequency content and complexity of the crustal resonances is well matched. We will show that this is not the case for explosions. The fit at BKS in Figure 16c is not as close in detail, but there are certainly hints of the arrival of crustal resonances. Again the period and complexity of the resonances is well matched. The fit at ALQ in 16d is again remarkable. Deterministic features associated with the crustal resonances are very clear. At the last three stations, GOL, LUB and LON., the matches are only average, but as before the period and complexity of the resonance phases are well modeled.

A similar comparison between synthetics and data for the explosion observations is shown in Figures 17a to h. In the earthquake calculations, the source depth was set at 8 km and for the explosion at 1 km. It was found, however, that variations in source depth of this order have almost no effect on the  $P_{n1}$  synthetics. The reason is that the travel times of the rays can be expressed as

$$T = pr + \sum h_i q_i$$

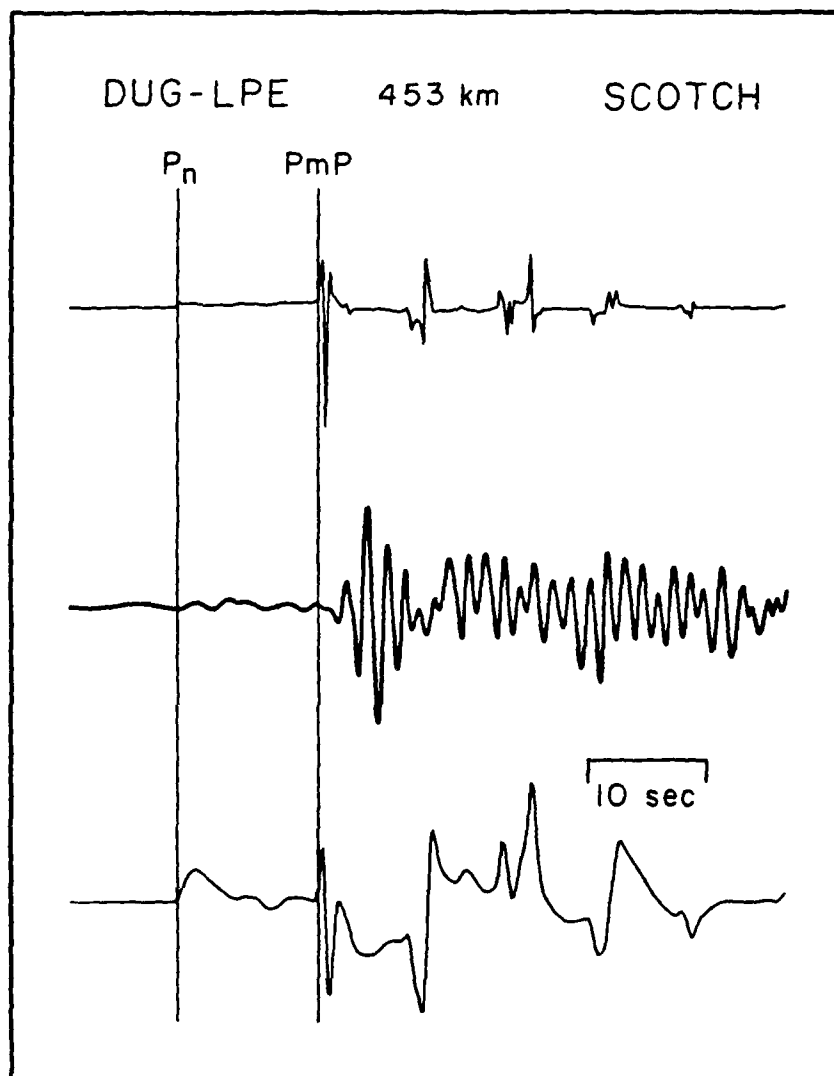


Figure 17a. A comparison between observed and synthetic  $P_{n1}$  records of the NTS events. The Green's function is shown at the top, the data in the center and the synthetic at the bottom. The vertical lines show the arrival of  $P_n$  and  $P_{mP}$ .

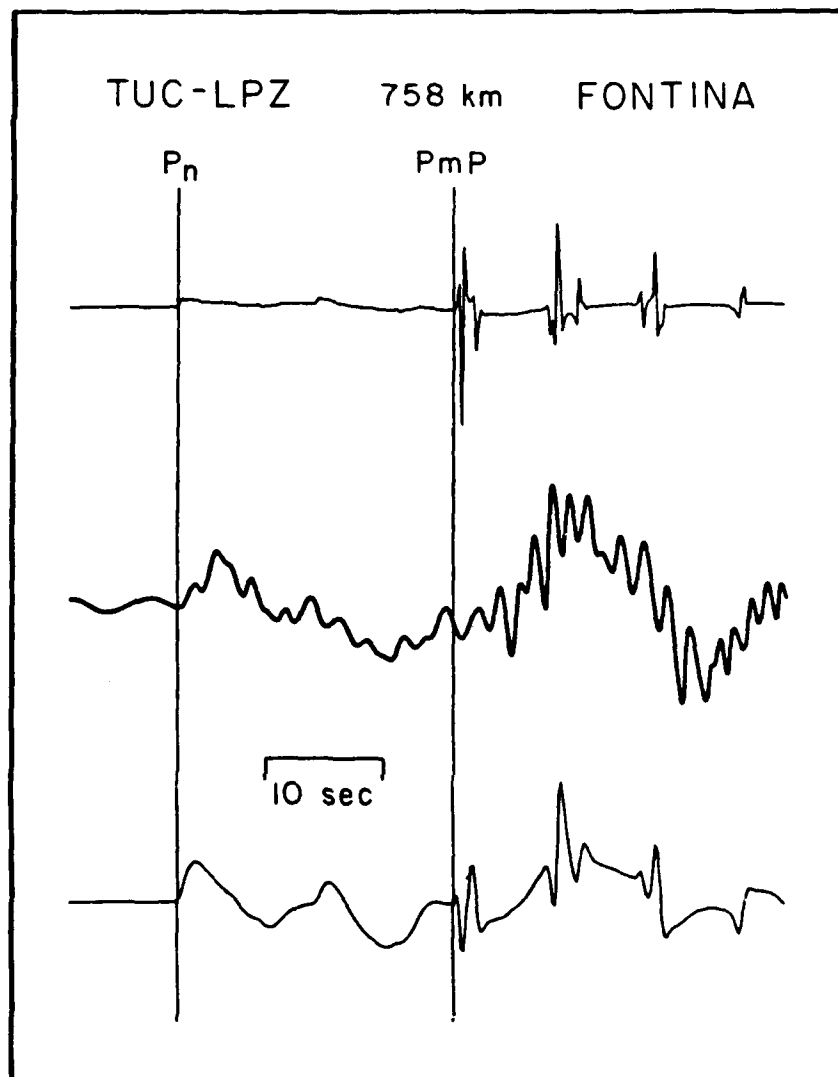


Figure 17b.

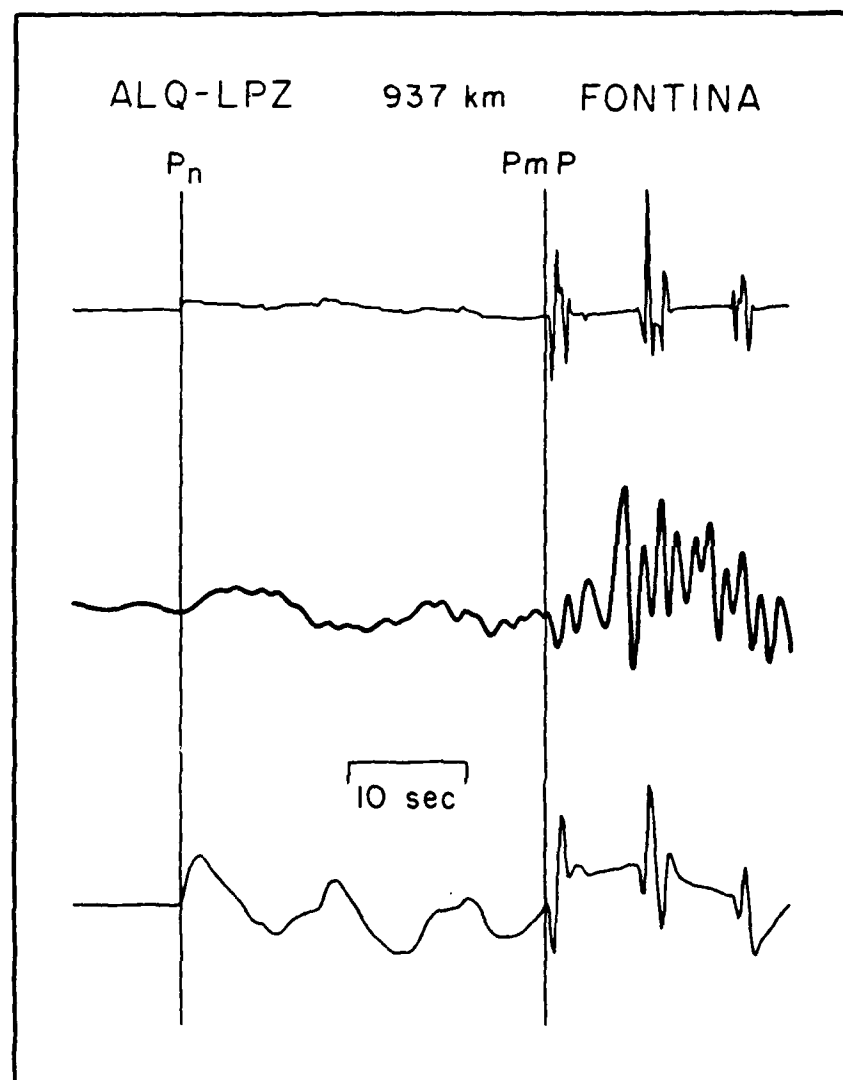


Figure 17c.

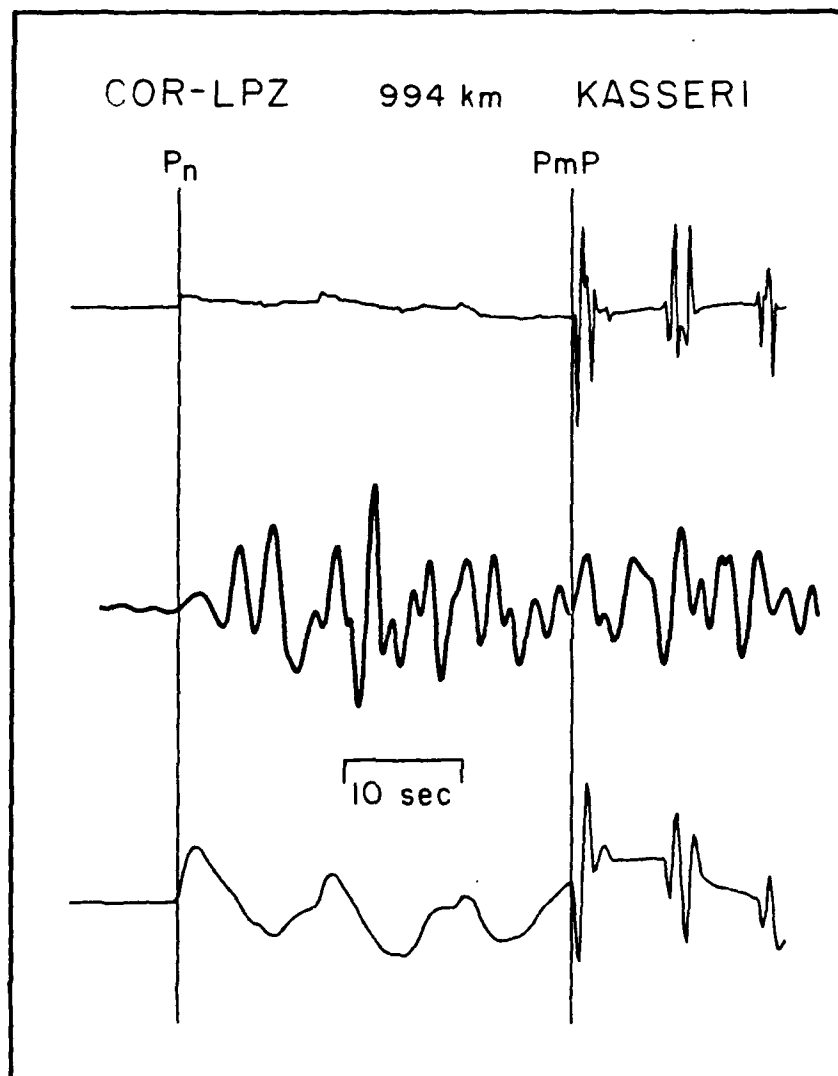


Figure 17d.

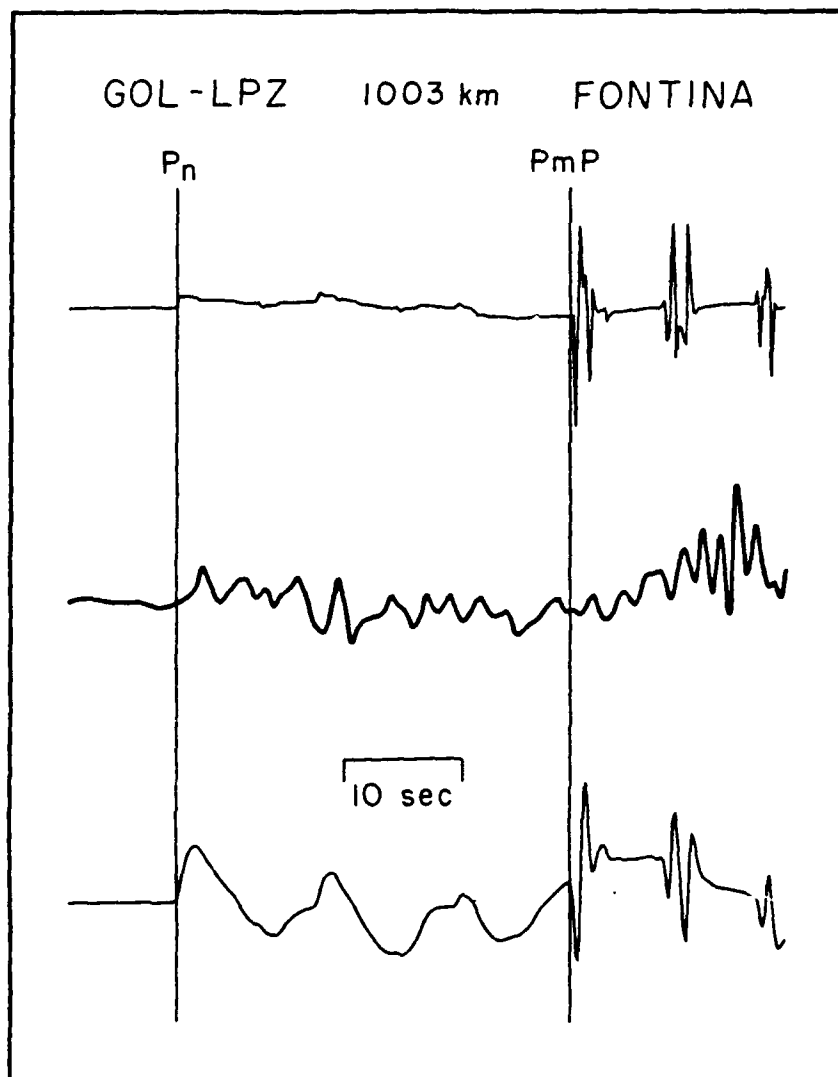


Figure 17e.



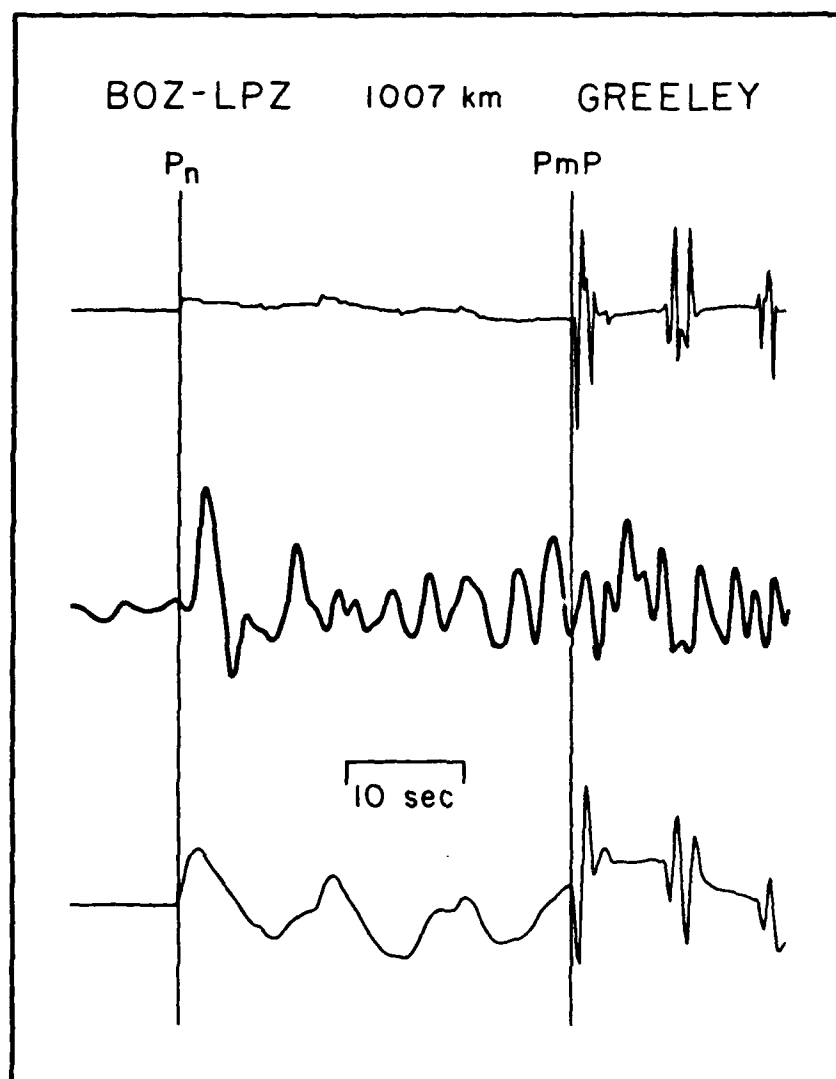


Figure 17f.

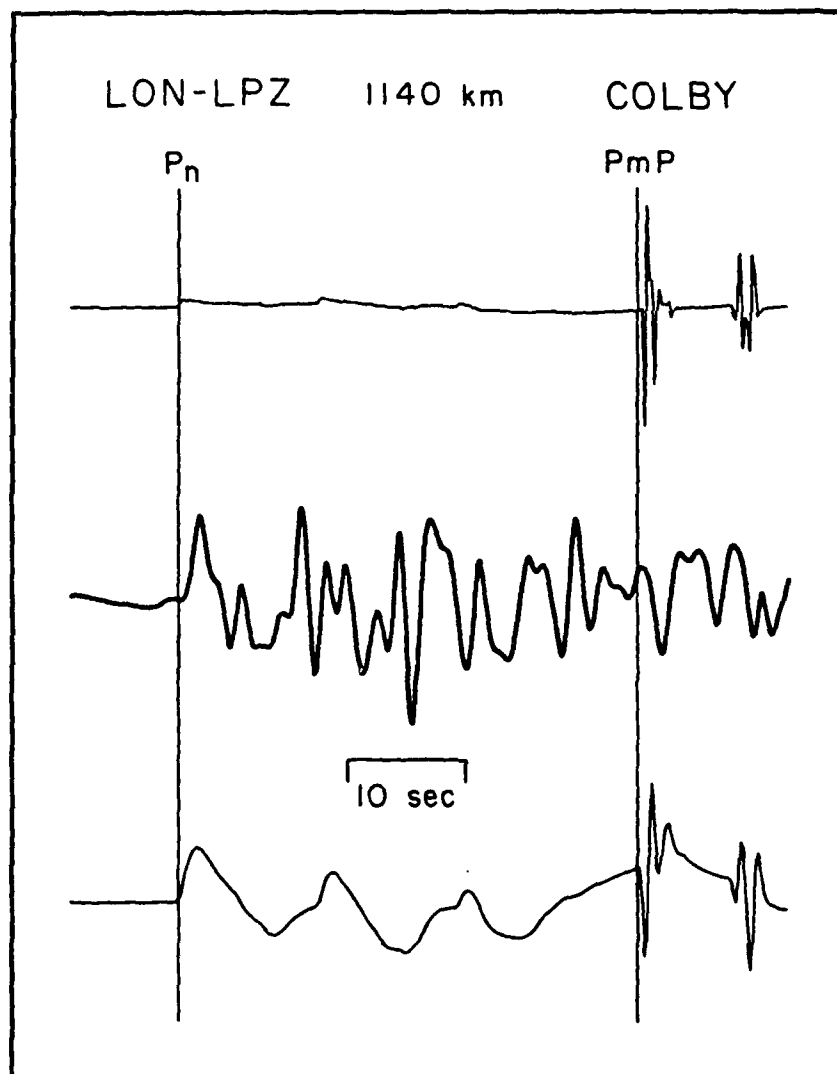


Figure 17g.

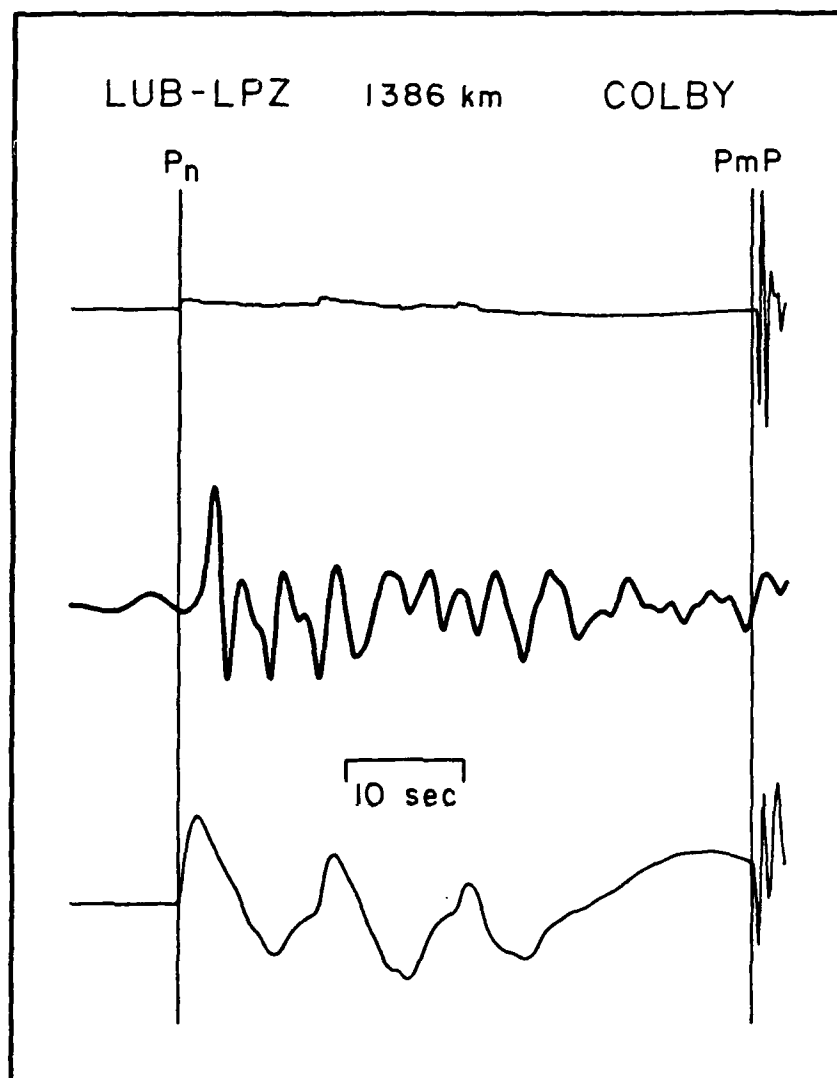


Figure 17h.

where  $p$  and  $q$  are horizontal and vertical slowness,  $r$  is horizontal range and  $h$  is the vertical extent of the "i"th ray leg. As  $r$  becomes long with respect to the  $h$ 's the vertical slownesses become very small. A perturbation in depth would simply advance or delay rays by  $qdh$ . For a perturbation of 10 km or so, this is a very small number. We will discuss the effects of depth perturbation further in the following section. The source used in the explosion calculations is the same one used in equalizing the explosion records in the seismic section (Burger et al., 1988). The synthetic predictions shown in Figure 17 must certainly be considered a failure given the high success at predicting fine details and general complexity and period of the resonance phases in the earthquake records. The synthetics are much too simple in character and in most cases too low in frequency content to explain the observations. This is apparently true for  $P_n$  as well as the crustal resonance phases. The modeling formalism has broken down. We illustrate the reason for this in the final section.

### IMPROVED METHODS FOR COMPUTING $P_{n1}$

It has been noted several times that the simple, layer over a half space model used to compute the Green's functions fails to predict any strong source depth dependence. Yet such effects would intuitively be expected to occur. In Figure 18, we compare the Helmberger and Engen (1980) crust model to a realistic crustal model for NTS. The top of the model is based on the modeling studies of near field data utilized by Burger et al. (1987). A slight crustal gradient down to the Moho has been added. The simple model does not contain the drop in velocity by a factor of about 3 which is well known to exist at the earth's surface. It is clear that the long period response of the two models should be just about the same. However at short periods, the waves will react to the strong gradient. Since the velocity in the top of the realistic model is much lower, rays will be bent toward the vertical, the details of mode conversion will change markedly and the relative timing of the rays will be altered. It would be desirable to simulate these effects exactly using a purely theoretical approach. However, it is impractical to continue to use generalized rays to do so because of the large number of interfaces involved. A wavenumber integration would be possible, but this method requires extensive computing to carry the calculations to high frequency. The goal of this discussion is just to explain the breakdown in the  $P_{n1}$  computing methodology, so we will use a semi-empirical approach to correcting for the effects of the surface gradient. The results we present are probably not highly accurate, so we intend to test them further in later work.

The physical effect of the strong near surface velocity gradient will be to cause the depth phases to develop more strongly at shorter ranges than in

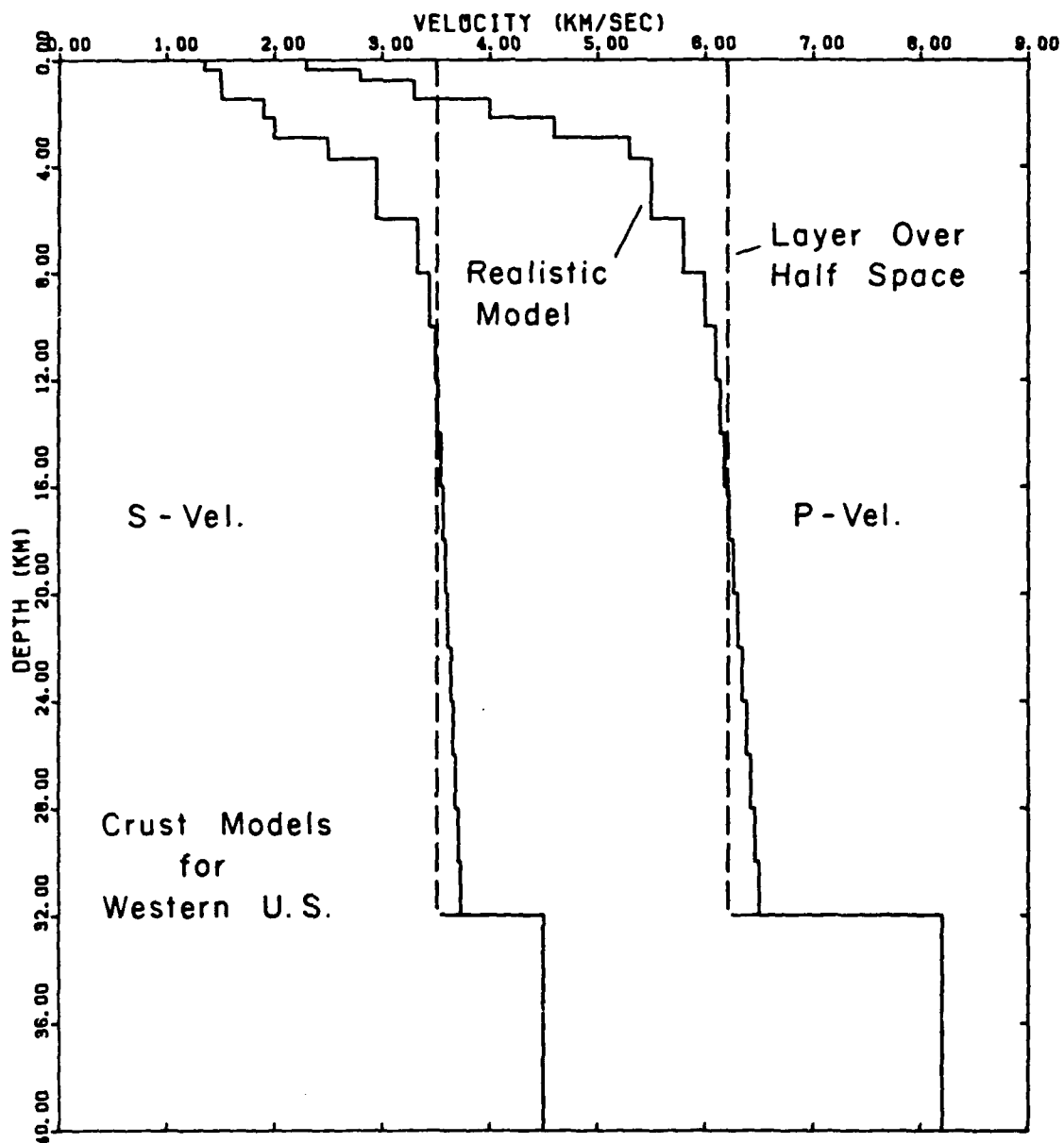


Figure 18. A comparison between a realistic and a layer over a half space crustal model for the western U.S.

the layer over a half space model. This suggests that we might wish to use an appropriate observed record from regional ranges as an effective source. We would like to select this record so that it contains the effects of the source time history, the free surface interaction, the instrument and attenuation. We would like the rest of the propagation effects on the pulse shape to be as minimal as possible. Likely candidate records are found at regional distances where the first arrival has penetrated the low velocity zone and begun to turn against the upper mantle gradient as shown in Figure 4. Two such observed first arrivals are shown at the top of Figure 19. The Caliente earthquake record from LON. (1213 km) is shown on the left and the COLBY explosion record from LUB (1386 km) is shown on the right. These signals appear very much like teleseismic records implying that the response of the earth away from the source is very much like a delta function. In the second row of the figure are shown P waves from beyond  $30^\circ$  for the two events. At these ranges the P waves turn in the smooth lower mantle and the response of the earth is known to be very well approximated by a delta function. The high correlation of the first and second row traces is clear. In the bottom row are synthetic traces appropriate for  $30^\circ$  computed using simple plane wave theory. The P and sP arrivals typical of a shallow strike slip earthquake are indicated on the left. It seems clear that the free surface phases are almost completely developed in the LON. record from Caliente. It is interesting to note that the LON. record appears more attenuated than the OGD record. This could be a manifestation of the low Q in the LVZ where the LON. pulse spent a larger portion of time. The synthetic for COLBY was computed using the structure shown in Figure 18. The P and pP phases are identified. Again it seems clear that the free surface interaction has developed completely by the range of LUB, and that the LUB P wave should make a reasonable effective source. We

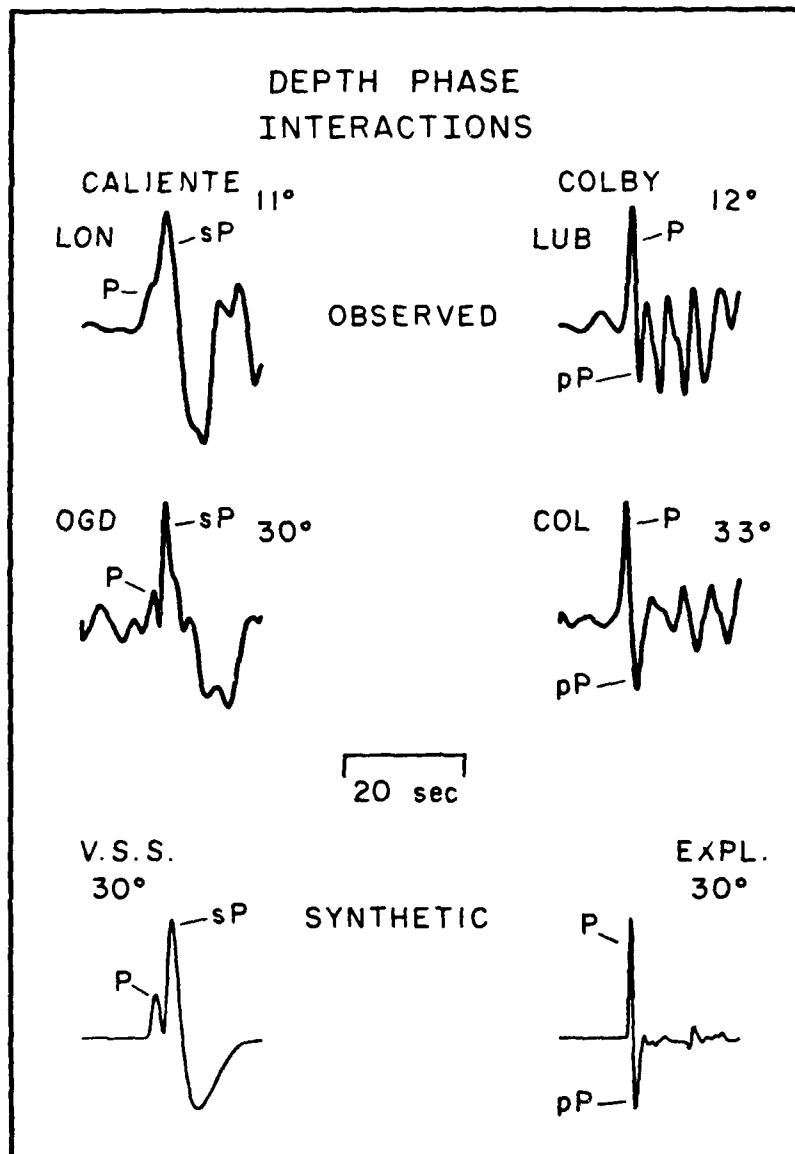


Figure 19. Observed records for the Caliente earthquake and Colby explosion at regional (top) and teleseismic (center) ranges compared to teleseismic synthetics (bottom).



wish also to note the additional ringing in the observed explosion records after pP which is not present in the synthetic. We shall discuss the possible causes for this later.

Computation of a synthetic seismogram using an effective source is relatively simple. Most of the phenomena usually represented by operators are present in the effective source time history. We need only convolve it with the Green's function for the earth. Using this approach, we repeat the calculation of explosion  $P_{n1}$ 's shown in Figure 17. The results are shown in Figure 20a through h. The new comparison of data and synthetic for DUG is shown in 20a. As before, the predicted Green's function is at the top. This time we show the effective source windowed from the LUB record at the right. The window used to extract the pulse was a trapezoid with 5 s edges. The improvement in the correlation between data and synthetic is quite strong. The first crustal resonance phase now has the appropriate frequency content and the general complexity of the  $P_g$  is matched to a much higher degree. The later crustal resonance phases are too large in the synthetics, but this is not surprising given the crudeness of our approach for correcting for depth effects. Here and in the later comparisons, the  $P_n$  is now matched much better. The match at TUC, ALQ and GOL are again better though problems with the amplitude of the later resonances remain. The record at COR is poorly matched though this is a very poor station site. At BOZ, the change in frequency content at the PmP time is matched and at LON. and LUB, we see the change in P to PmP timing due to the effect of the positive mantle gradient just as before. The result of this simple numerical experiment is to show

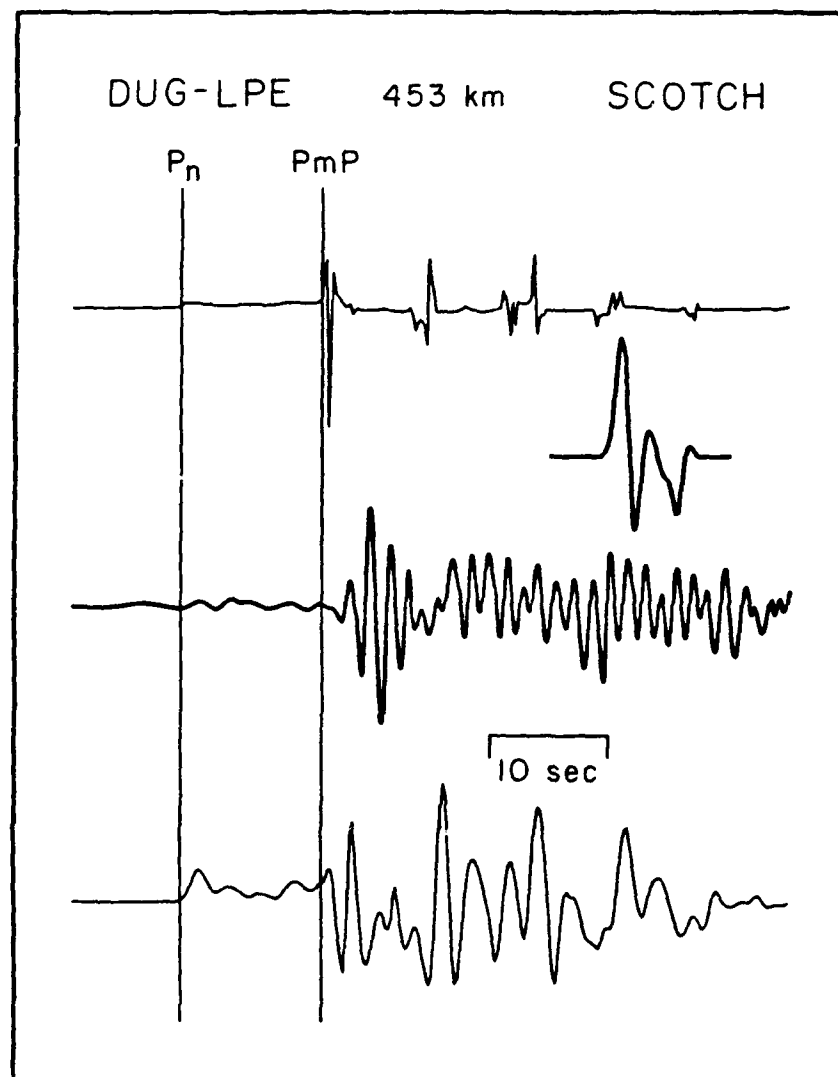


Figure 20a. A comparison between observed and synthetic  $P_{n1}$  records of the NTS events. The synthetics are computed using the effective source approach. The Green's function is shown at the top, the effective source to the right, the data in the center and the synthetic at the bottom. The vertical lines show the arrival of  $P_n$  and  $P_{mP}$ .

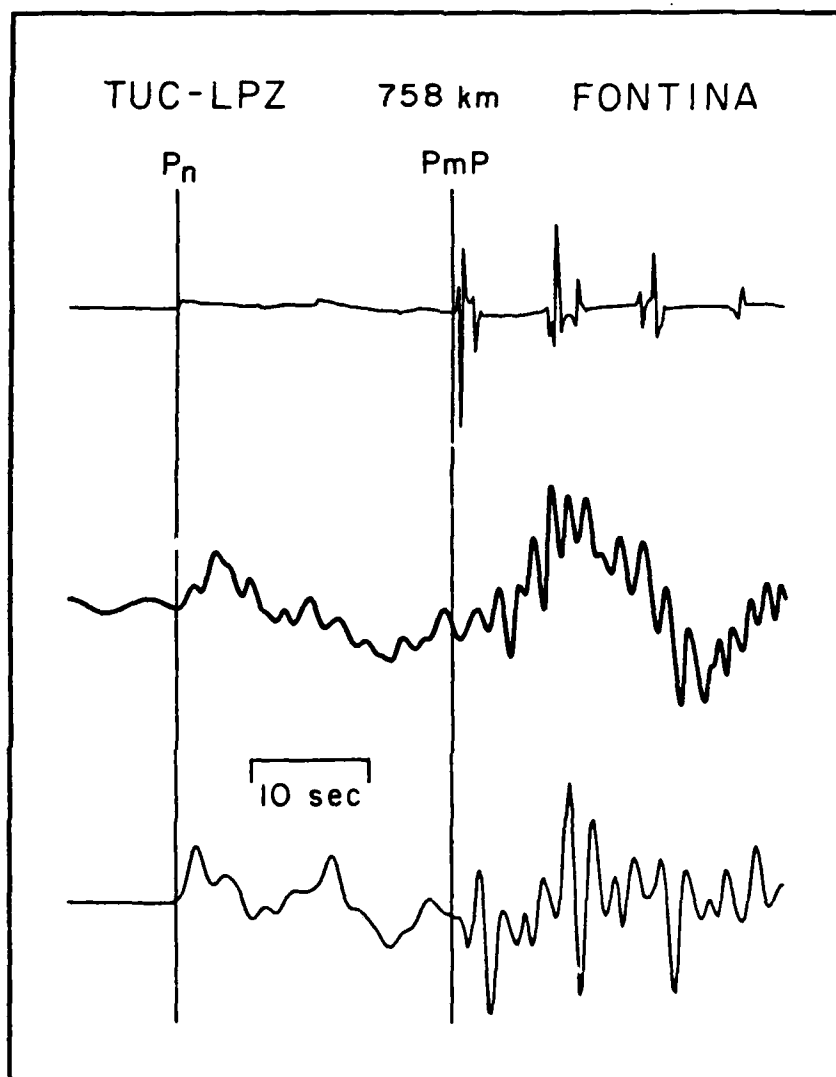


Figure 20b.

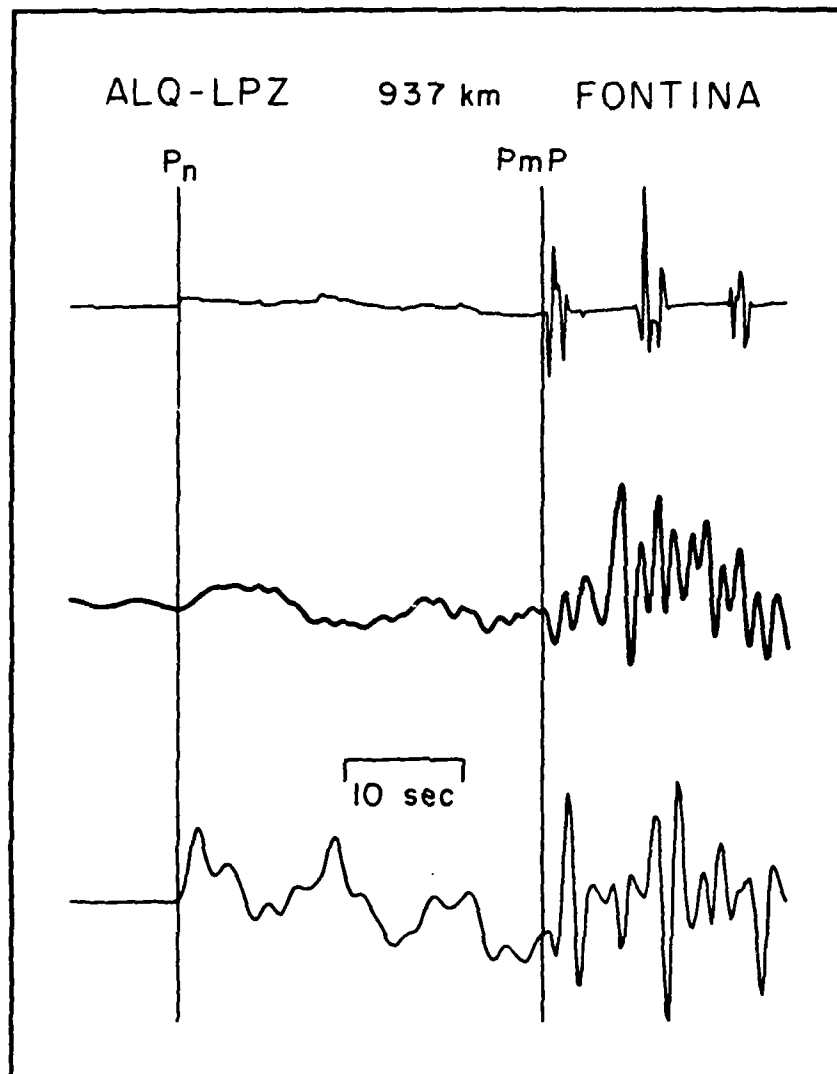


Figure 20c.

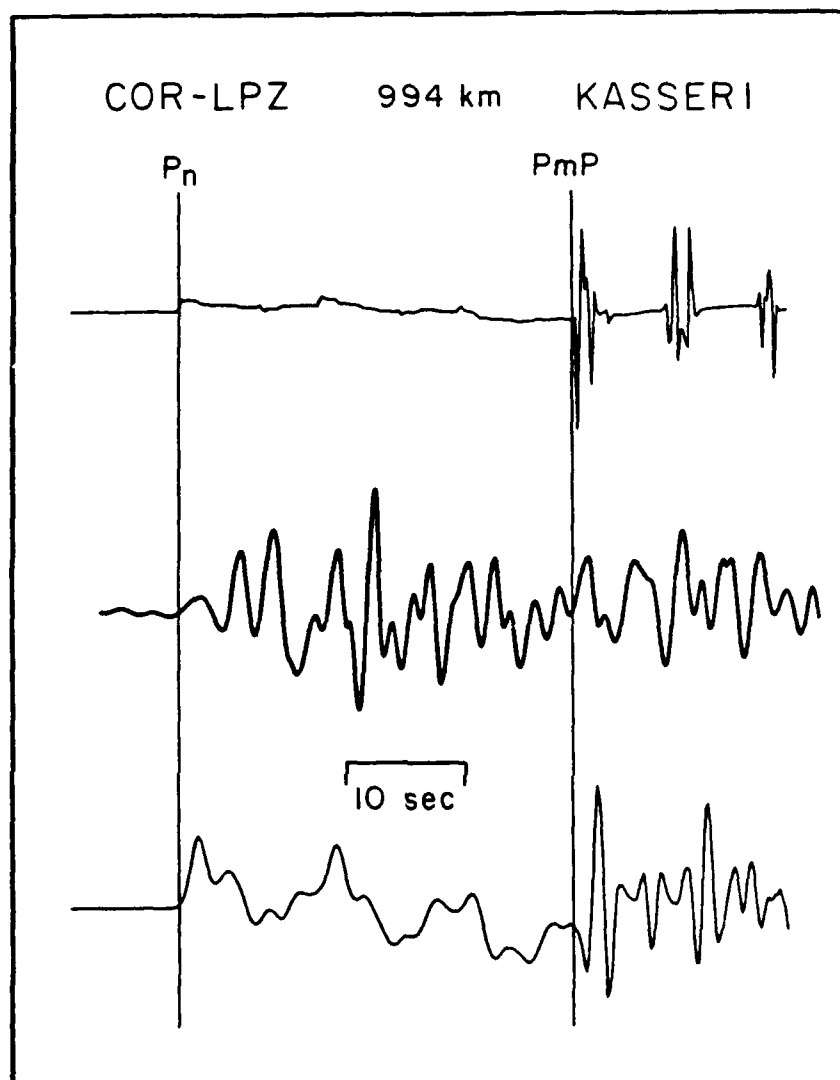


Figure 20d.

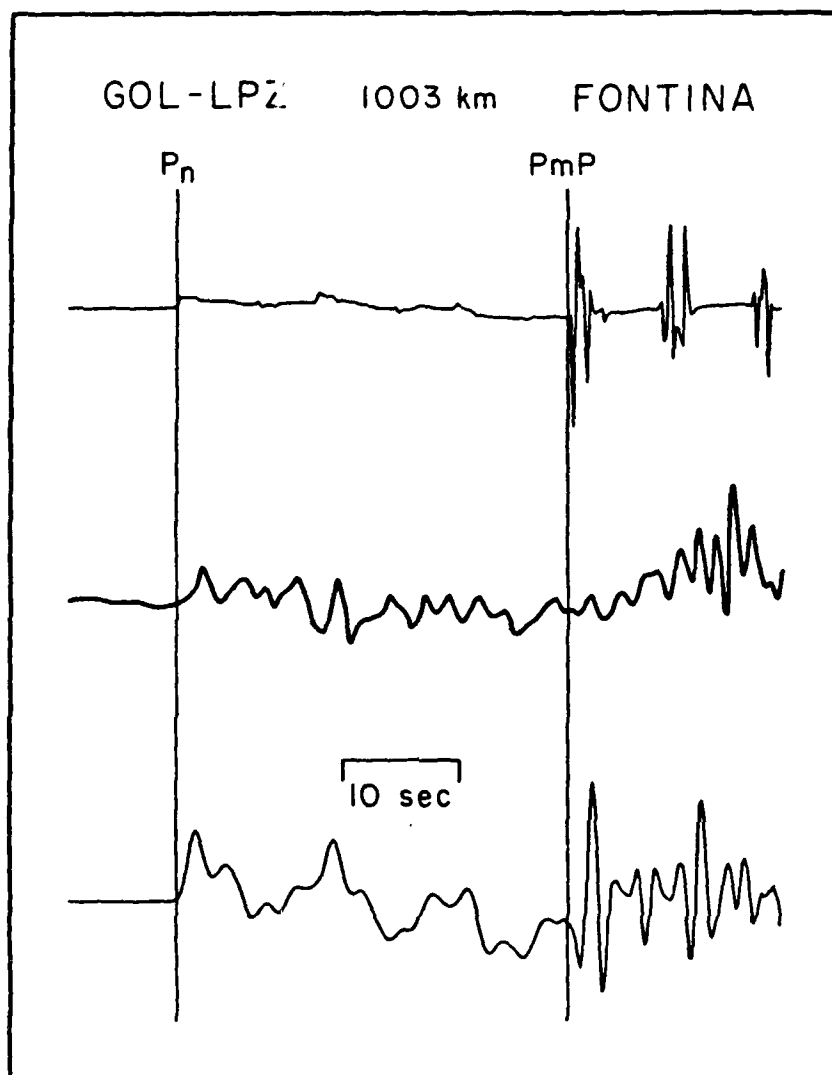


Figure 20e.

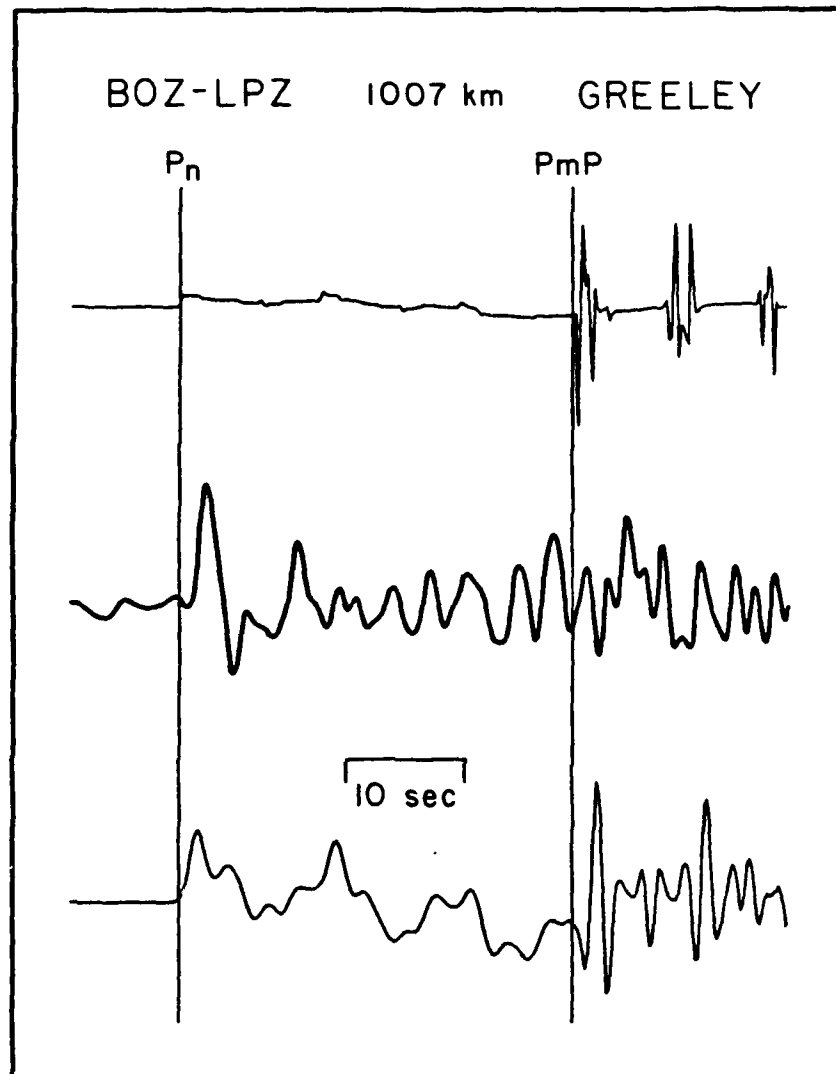


Figure 20f.

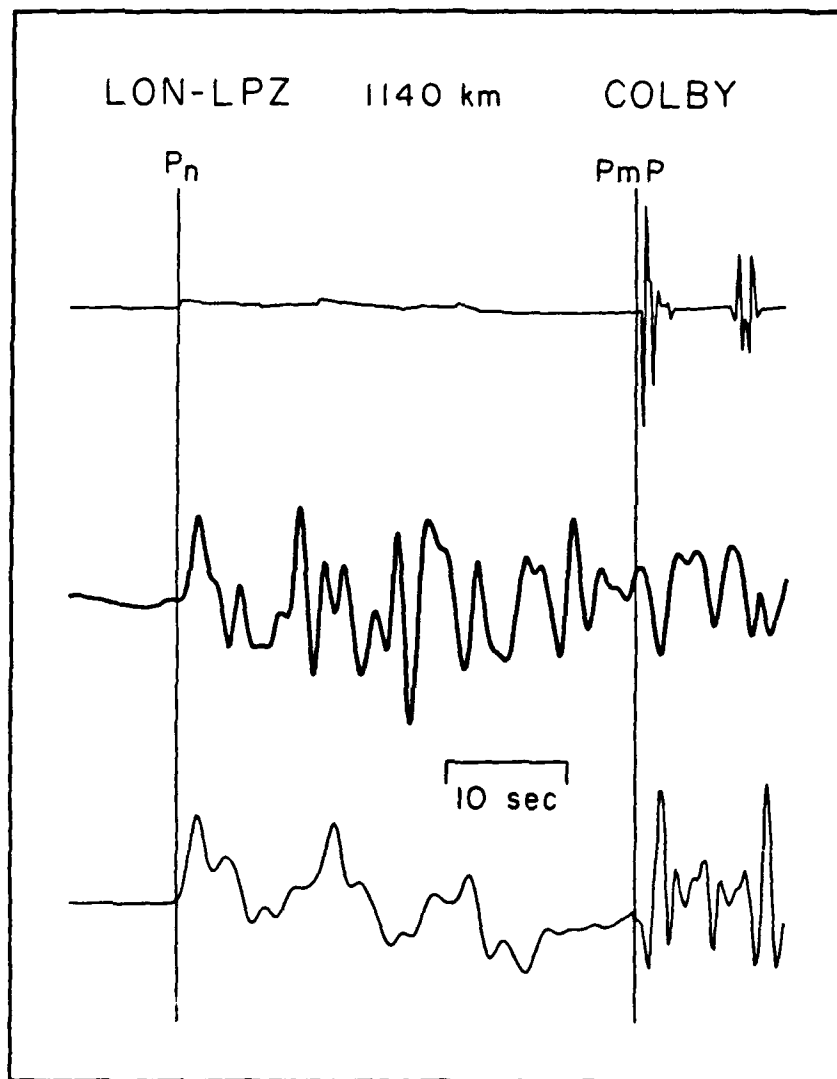


Figure 20g.



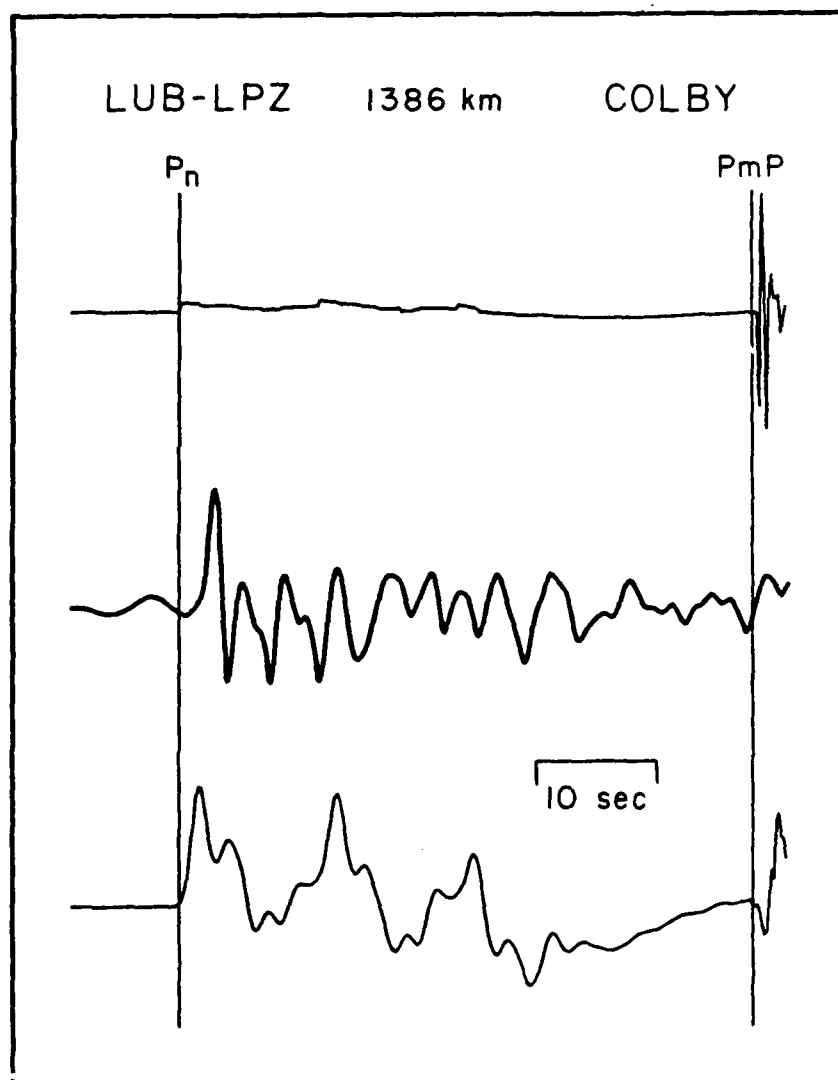


Figure 20h.

that explosion  $P_{n1}$ 's are much more strongly sensitive to depth than layer over half space calculations indicate and that we may have a good chance of basing a depth discriminant on them.

## DISCUSSION

Since only long period data have been explicitly collected and modeled to this point in the study, no explicit new high frequency discriminants have been developed. Yet, important progress has been made. It has always been somewhat of a mystery why regional  $P_g$  typically has such a long duration. Now that it is clear that  $P_g$  is actually built up from a sequence of crustal resonance phases, this phenomenon is simple to explain. If each successive resonance carries with it a typical amount of high frequency scattered energy, the long duration and complexity of  $P_g$  would be a natural consequence. Also we have demonstrated that the crustal resonance phases for earthquakes are deterministic to relatively short periods. This means that, except for the effects of shallow structure on very shallow sources, the response of the earth is well behaved, and, at least in the western U.S., we could reliably predict for any observed short period signal a corresponding long period envelope signal. From this envelope signal, we could determine within a second or two when important crustal resonances are arriving. By carefully processing and analyzing information from these windows, we may be able to develop the required new levels of discrimination accuracy. How these discriminants would be designed will be the subject of future work. The answer may be as simple as taking the ratio of the power in the first to the second resonance phase.

The strong improvement in the match of data and synthetics for explosions between Figures 17 and 20 indicates that a strong effort to base a depth discriminant on crustal resonance phases should be undertaken. However, it is unclear how to proceed in designing this discriminant. It may turn out that

the durations of explosion crustal resonances will simply be shorter because of the reduced time between the direct and surface reflected arrivals. There are many unstable scattering processes which are significant at high frequency, on the other hand, so it may be that only some average properties of the signals will be diagnostic. In discussing Figure 19, we noted that observed explosion signals often have a coda which is not predicted by realistic plane layered models. Some three dimensional scattering phenomena is clearly indicated.

## CONCLUSIONS

In this investigation we have made important progress in understanding the substructure of the regional phase  $P_g$ . Through synthetic seismogram analysis we have found that the complete arrival contains a sequence of subarrivals which we have named crustal resonance phases. In terms of generalized rays, successive crustal resonance phases are generated to some extent by increasing order of the number of reverberations the rays have in the crust. However, we have investigated the composition of the first two resonance phases in detail and found that the first is generated by  $PmP$ ,  $SmS$  and their surface reflections while the second is generated by several first order converted phases. It thus appears that each reverberation in the crust can cause more than one resonance phase. Profiles of regional data from explosions and an earthquake have been collected and modeled with synthetic seismograms. The earthquake data show that the crustal resonance phases are stable and deterministic up to periods as short as 1 second. The explosion data shows that the regional  $P_g$  signal is much more sensitive to source depth than layer over a half space calculations would indicate.

## REFERENCES

- Blandford, R., "Seismic event discrimination", *Bull. Seism. Soc. Am.*, 72, S69-S87, 1982.
- Burdick, L. J. and D. V. Helmberger, "The upper mantle P velocity structure of the Western United States", *J. Geophys. Res.*, 83, 1699-1712, 1978.
- Burdick, L. J. and J. A. Orcutt, "A comparison of the generalized ray and reflectivity methods of waveform synthesis", *Geophys. J. R. astr. Soc.*, 58, 261-278, 1979.
- Burger, R. W., T. Lay and L. J. Burdick, "Average Q and yield estimates from the Pahute Mesa test site", *Bull. Seism. Soc. Am.*, 77, 1274-1294, 1987.
- Helmberger, D. V., "On the structure of the low velocity zone", *Geophys. J. Roy. astr. Soc.*, 34, 251-263, 1973.
- Helmberger, D. V., and G. R. Engen, "Modeling the long period body waves from shallow earthquakes at regional ranges", *Bull. Seism. Soc. Am.*, 70, 1699-1714, 1980.
- Langston, C. A., and D. V. Helmberger, "Rayleigh waves from NTS to Tucson", *Bull. Seism. Soc. Am.*, 64, 1919-1929, 1974.
- Murphy, J. R., "Seismic source functions and magnitude determinations of underground nuclear detonations", *Bull. Seism. Soc. Am.*, 67, 135-156, 1977.
- Murphy, J. R. and T. J. Bennett, "A discrimination analysis of short period regional seismic data recorded at Tonto Forest Observatory", *Bull. Seism. Soc. Am.*, 72, 1351-1366, 1982.
- Oliver, J. and M. Major, "Leaking modes and the PL phase", *Bull. Seism. Soc. Am.*, 50, 165-180, 1960.
- Pakiser, L. C., "Structure of the crust and upper mantle in the western U.S.", *J. Geophys. Res.*, 68, 5747-5756, 1963.
- Pomeroy, P. W., W. J. Best and T. V. McEvelly, "Test band treaty verification with regional data - a review", *Bull. Seism. Soc. Am.*, 72, S89-S129, 1982.
- Wallace, T. C., D. V. Helmberger and G. R. Engen, "Evidence of tectonic release from underground nuclear explosions in long period P waves", *Bull. Seism. Soc. Am.*, 73, 593-614, 1983.
- Wallace, T. C., D. V. Helmberger and G. R. Mellman, "A technique for the inversion of regional data in source parameter studies", *J. Geophys. Res.*, 86, 1679-1685, 1981.

CONTRACTORS (United States)

Professor Keiiti Aki  
Center for Earth Sciences  
University of Southern California  
University Park  
Los Angeles, CA 90089-0741

Professor Charles B. Archambeau  
Cooperative Institute for Resch  
in Environmental Sciences  
University of Colorado  
Boulder, CO 80309

Dr. Thomas C. Bache Jr.  
Science Applications Int'l Corp.  
10210 Campus Point Drive  
San Diego, CA 92121 (2 copies)

Dr. Douglas R. Baumgardt  
Signal Analysis & Systems Div.  
ENSCO, Inc.  
5400 Port Royal Road  
Springfield, VA 22151-2388

Dr. S. Bratt  
Science Applications Int'l Corp.  
10210 Campus Point Drive  
San Diego, CA 92121

Dr. Lawrence J. Burdick  
Woodward-Clyde Consultants  
P.O. Box 93245  
Pasadena, CA 91109-3245 (2 copies)

Professor Robert W. Clayton  
Seismological Laboratory/Div. of  
Geological & Planetary Sciences  
California Institute of Technology  
Pasadena, CA 91125

Dr. Vernon F. Cormier  
Department of Geology & Geophysics  
U-45, Room 207  
The University of Connecticut  
Storrs, Connecticut 06268

Dr. Zoltan A. Der  
ENSCO, Inc.  
5400 Port Royal Road  
Springfield, VA 22151-2388

Professor John Ferguson  
Center for Lithospheric Studies  
The University of Texas at Dallas  
P.O. Box 830688  
Richardson, TX 75083-0688

Professor Stanley Flatte'  
Applied Sciences Building  
University of California, Santa Cruz  
Santa Cruz, CA 95064

Professor Steven Grand  
Department of Geology  
245 Natural History Building  
1301 West Green Street  
Urbana, IL 61801

Professor Roy Greenfield  
Geosciences Department  
403 Deike Building  
The Pennsylvania State University  
University Park, PA 16802

Professor David G. Harkrider  
Seismological Laboratory  
Div of Geological & Planetary Sciences  
California Institute of Technology  
Pasadena, CA 91125

Professor Donald V. Helmberger  
Seismological Laboratory  
Div of Geological & Planetary Sciences  
California Institute of Technology  
Pasadena, CA 91125

Professor Eugene Herrin  
Institute for the Study of Earth  
& Man/Geophysical Laboratory  
Southern Methodist University  
Dallas, TX 75275

Professor Robert B. Herrmann  
Department of Earth & Atmospheric  
Sciences  
Saint Louis University  
Saint Louis, MO 63156

Professor Lane R. Johnson  
Seismographic Station  
University of California  
Berkeley, CA 94720

Professor Thomas H. Jordan  
Department of Earth, Atmospheric  
and Planetary Sciences  
Mass Institute of Technology  
Cambridge, MA 02139

Dr. Alan Kafka  
Department of Geology &  
Geophysics  
Boston College  
Chestnut Hill, MA 02167



Professor Leon Knopoff  
University of California  
Institute of Geophysics  
& Planetary Physics  
Los Angeles, CA 90024

Professor Charles A. Langston  
Geosciences Department  
403 Deike Building  
The Pennsylvania State University  
University Park, PA 16802

Professor Thorne Lay  
Department of Geological Sciences  
1006 C.C. Little Building  
University of Michigan  
Ann Harbor, MI 48109-1063

Dr. Randolph Martin III  
New England Research, Inc.  
P.O. Box 857  
Norwich, VT 05055

Dr. Cary McCartor  
Mission Research Corp.  
735 State Street  
P.O. Drawer 719  
Santa Barbara, CA 93102 (2 copies)

Professor Thomas V. McEvelly  
Seismographic Station  
University of California  
Berkeley, CA 94720

Dr. Keith L. McLaughlin  
S-CUBED,  
A Division of Maxwell Laboratory  
P.O. Box 1620  
La Jolla, CA 92038-1620

Professor William Menke  
Lamont-Doherty Geological Observatory  
of Columbia University  
Palisades, NY 10964

Professor Brian J. Mitchell  
Department of Earth & Atmospheric  
Sciences  
Saint Louis University  
Saint Louis, MO 63156

Mr. Jack Murphy  
S-CUBED  
A Division of Maxwell Laboratory  
11800 Sunrise Valley Drive  
Suite 1212  
Reston, VA 22091 (2 copies)

Professor J. A. Orcutt  
Institute of Geophysics and Planetary  
Physics, A-205  
Scripps Institute of Oceanography  
Univ. of California, San Diego  
La Jolla, CA 92093

Professor Keith Priestley  
University of Nevada  
Mackay School of Mines  
Reno, Nevada 89557

Professor Charles G. Sammis  
Center for Earth Sciences  
University of Southern California  
University Park  
Los Angeles, CA 90089-0741

Dr. Jeffrey L. Stevens  
S-CUBED,  
A Division of Maxwell Laboratory  
P.O. Box 1620  
La Jolla, CA 92038-1620

Professor Brian Stump  
Institute for the Study of Earth & Man  
Geophysical Laboratory  
Southern Methodist University  
Dallas, TX 75275

Professor Ta-liang Teng  
Center for Earth Sciences  
University of Southern California  
University Park  
Los Angeles, CA 90089-0741

Professor M. Nafi Toksoz  
Earth Resources Lab  
Dept of Earth, Atmospheric and  
Planetary Sciences  
Massachusetts Institute of Technology  
42 Carleton Street  
Cambridge, MA 02142

Professor Terry C. Wallace  
Department of Geosciences  
Building #11  
University of Arizona  
Tucson, AZ 85721

Professor Francis T. Wu  
Department of Geological Sciences  
State University of New York  
At Binghamton  
Vestal, NY 13901

Rong Song Jih  
Teledyne Geotech  
314 Montgomery Street  
Alexandria, Virginia 22314

OTHERS (United States)

Dr. Monem Abdel-Gawad  
Rockwell Internat'l Science Center  
1049 Camino Dos Rios  
Thousand Oaks, CA 91360

Professor Shelton S. Alexander  
Geosciences Department  
403 Deike Building  
The Pennsylvania State University  
University Park, PA 16802

Dr. Muawia Barazangi  
Geological Sciences  
Cornell University  
Ithaca, NY 14853

J. Barker  
Department of Geological Sciences  
State University of New York  
at Binghamton  
Vestal, NY 13901

Mr. William J. Best  
907 Westwood Drive  
Vienna, VA 22180

Dr. N. Biswas  
Geophysical Institute  
University of Alaska  
Fairbanks, AK 99701

Dr. G. A. Bollinger  
Department of Geological Sciences  
Virginia Polytechnical Institute  
21044 Derring Hall  
Blacksburg, VA 24061

Dr. James Bulau  
Rockwell Int'l Science Center  
1049 Camino Dos Rios  
P.O. Box 1085  
Thousand Oaks, CA 91360

Mr. Roy Burger  
1221 Serry Rd.  
Schenectady, NY 12309

Dr. Robert Burridge  
Schlumberger-Doll Resch Ctr.  
Old Quarry Road  
Ridgefield, CT 06877

Science Horizons, Inc.  
ATTN: Dr. Theodore Cherry  
710 Encinitas Blvd., Suite 101  
Encinitas, CA 92024 (2 copies)

Professor Jon F. Claerbout  
Professor Amos Nur  
Dept. of Geophysics  
Stanford University  
Stanford, CA 94305 (2 copies)

Dr. Anton W. Dainty  
AFGL/LWH  
Wright-Patterson AFB, MA 01731

Professor Adam Dziewonski  
Hoffman Laboratory  
Harvard University  
20 Oxford St.  
Cambridge, MA 02138

Professor John Ebel  
Dept of Geology & Geophysics  
Boston College  
Chestnut Hill, MA 02167

Dr. Alexander Florence  
SRI International  
333 Ravenwood Avenue  
Menlo Park, CA 94025-3493

Dr. Donald Forsyth  
Dept. of Geological Sciences  
Brown University  
Providence, RI 02912

Dr. Anthony Gangi  
Texas A&M University  
Department of Geophysics  
College Station, TX 77843

Dr. Freeman Gilbert  
Institute of Geophysics &  
Planetary Physics  
Univ. of California, San Diego  
P.O. Box 109  
La Jolla, CA 92037

Mr. Edward Giller  
Pacific Sierra Research Corp.  
1401 Wilson Boulevard  
Arlington, VA 22209

Dr. Jeffrey W. Givens  
Sierra Geophysics  
11255 Kirkland Way  
Kirkland, WA 98033

Dr. Henry L. Gray  
Associate Dean of Dedman College  
Department of Statistical Sciences  
Southern Methodist University  
Dallas, TX 75275

Professor F.K. Lamb  
University of Illinois at  
Urbana-Champaign  
Department of Physics  
1110 West Green Street  
Urbana, IL 61801

Dr. Arthur Lerner-Lam  
Lamont-Doherty Geological Observatory  
of Columbia University  
Palisades, NY 10964

Dr. L. Timothy Long  
School of Geophysical Sciences  
Georgia Institute of Technology  
Atlanta, GA 30332

Dr. Peter Malin  
University of California at Santa Barbara  
Institute for Central Studies  
Santa Barbara, CA 93106

Dr. George R. Mellman  
Sierra Geophysics  
11255 Kirkland Way  
Kirkland, WA 98033

Dr. Bernard Minster  
Institute of Geophysics and Planetary  
Physics, A-205  
Scripps Institute of Oceanography  
Univ. of California, San Diego  
La Jolla, CA 92093

Dr. Geza Nagy  
SRI International  
333 Ravenswood Avenue  
Menlo Park, CA 94025-3493

Dr. Jack Oliver  
Department of Geology  
Cornell University  
Ithaca, NY 14850

Dr. Robert Phinney/Dr. F.A. Dahlen  
Dept of Geological  
Geophysical Sci. University  
Princeton University  
Princeton, NJ 08540 (2 copies)

Professor Paul G. Richards  
Lamont-Doherty Geological  
Observatory of Columbia Univ.  
Palisades, NY 10964

Dr. Norton Rimer  
S-CUBED  
A Division of Maxwell Laboratory  
P.O. 1620  
La Jolla, CA 92038-1620

Wilmer Rivers  
Teledyne Geotech  
314 Montgomery Street  
Alexandria VA 22314

Professor Larry J. Ruff  
Department of Geological Sciences  
1006 C.C. Little Building  
University of Michigan  
Ann Arbor, MI 48109-1063

Dr. Alan S. Ryall, Jr.  
Center of Seismic Studies  
1300 North 17th Street  
Suite 1450  
Arlington, VA 22209-2308 (4 copies)

Dr. David G. Simpson  
Lamont-Doherty Geological Observ.  
of Columbia University  
Palisades, NY 10964

Dr. Bob Smith  
Department of Geophysics  
University of Utah  
1400 East 2nd South  
Salt Lake City, UT 84112

Dr. S. W. Smith  
Geophysics Program  
University of Washington  
Seattle, WA 98195

Rondout Associates  
ATTN: Dr. George Sutton,  
Dr. Jerry Carter, Dr. Paul Pomeroy  
P.O. Box 224  
Stone Ridge, NY 12484 (4 copies)

Dr. L. Sykes  
Lamont Doherty Geological Observ.  
Columbia University  
Palisades, NY 10964

Dr. Pradeep Talwani  
Department of Geological Sciences  
University of South Carolina  
Columbia, SC 29208

Dr. R. B. Tittmann  
Rockwell International Science Center  
1049 Camino Dos Rios  
P.O. Box 1085  
Thousand Oaks, CA 91360

Weidlinger Associates  
ATTN: Dr. Gregory Wojcik  
620 Hansen Way, Suite 100  
Palo Alto, CA 94304

Professor John H. Woodhouse  
Hoffman Laboratory  
Harvard University  
20 Oxford St.  
Cambridge, MA 02138

Dr. Gregory B. Young  
ENSCO, Inc.  
5400 Port Royal Road  
Springfield, VA 22151-2388



OTHERS (FOREIGN)

Dr. Peter Basham  
Earth Physics Branch  
Geological Survey of Canada  
1 Observatory Crescent  
Ottawa, Ontario  
CANADA K1A 0Y3

Dr. Eduard Berg  
Institute of Geophysics  
University of Hawaii  
Honolulu, HI 96822

Dr. Michel Bouchon - Universite  
Scientifique et Medicale de Grenob  
Lab de Geophysique - Interne et  
Tectonophysique - I.R.I.G.M-B.P.  
38402 St. Martin D'Herès  
Cedex FRANCE

Dr. Hilmar Bungum/NTNF/NORSAR  
P.O. Box 51  
Norwegian Council of Science,  
Industry and Research, NORSAR  
N-2007 Kjeller, NORWAY

Dr. Michel Campillo  
I.R.I.G.M.-B.P. 68  
38402 St. Martin D'Herès  
Cedex, FRANCE

Dr. Kin-Yip Chun  
Geophysics Division  
Physics Department  
University of Toronto  
Ontario, CANADA M5S 1A7

Dr. Alan Douglas  
Ministry of Defense  
Blacknest, Brimpton,  
Reading RG7-4RS  
UNITED KINGDOM

Dr. Manfred Henger  
Fed. Inst. For Geosciences & Nat'l Res.  
Postfach 510153  
D-3000 Hannover 51  
FEDERAL REPUBLIC OF GERMANY

Dr. E. Husebye  
NTNF/NORSAR  
P.O. Box 51  
N-2007 Kjeller, NORWAY

Tormod Kvaerna  
NTNF/NORSAR  
P.O. Box 51  
N-2007 Kjeller, NORWAY

Mr. Peter Marshall, Procurement  
Executive, Ministry of Defense  
Blacknest, Brimpton,  
Reading FG7-4RS  
UNITED KINGDOM (3 copies)

Dr. Ben Menaheim  
Weizman Institute of Science  
Rehovot, ISRAEL 951729

Dr. Svein Mykkeltveit  
NTNF/NORSAR  
P.O. Box 51  
N-2007 Kjeller, NORWAY (3 copies)

Dr. Robert North  
Geophysics Division  
Geological Survey of Canada  
1 Observatory crescent  
Ottawa, Ontario  
CANADA, K1A 0Y3

Dr. Frode Ringdal  
NTNF/NORSAR  
P.O. Box 51  
N-2007 Kjeller, NORWAY

Dr. Jorg Schlittenhardt  
Federal Inst. for Geosciences & Nat'l Res.  
Postfach 510153  
D-3000 Hannover 51  
FEDERAL REPUBLIC OF GERMANY

University of Hawaii  
Institute of Geophysics  
ATTN: Dr. Daniel Walker  
Honolulu, HI 96822

FOREIGN CONTRACTORS

Dr. Ramon Cabre, S.J.  
c/o Mr. Ralph Buck  
Economic Consular  
American Embassy  
APO Miami, Florida 34032

Professor Peter Harjes  
Institute for Geophysik  
Rhur University/Bochum  
P.O. Box 102148 4630 Bochum 1  
FEDERAL REPUBLIC OF GERMANY

Professor Brian L.N. Kennett  
Research School of Earth Sciences  
Institute of Advanced Studies  
G.P.O. Box 4  
Canberra 2601  
AUSTRALIA

Dr. B. Massinon  
Societe Radiomana  
27, Rue Claude Bernard  
75005, Paris, FRANCE (2 copies)

Dr. Pierre Mechler  
Societe Radiomana  
27, Rue Claude Bernard  
75005, Paris, FRANCE

GOVERNMENT

Dr. Ralph Alewine III  
DARPA/NMRO  
1400 Wilson Boulevard  
Arlington, VA 22209-2308

Dr. Peter Basham  
Geological Survey of Canada  
1 Observatory Creseut  
Ottawa, Ontario  
CANADA K1A 0Y3

Dr. Robert Blandford  
DARPA/NMRO  
1400 Wilson Boulevard  
Arlington, VA 22209-2308

Sandia National Laboratory  
ATTN: Dr. H. B. Durham  
Albuquerque, NM 87185

Dr. Jack Evernden  
USGS-Earthquake Studies  
345 Middlefield Road  
Menlo Park, CA 94025

U.S. Geological Survey  
ATTN: Dr. T. Hanks  
Nat'l Earthquake Resch Center  
345 Middlefield Road  
Menlo Park, CA 94025

Dr. James Hannon  
Lawrence Livermore Nat'l Lab.  
P.O. Box 808  
Livermore, CA 94550

U.S. Arms Control & Disarm. Agency  
ATTN: Dick Morrow  
Washington, D.C. 20451

Paul Johnson  
ESS-4, Mail Stop J979  
Los Alamos National Laboratory  
Los Alamos, NM 87545

Ms. Ann Kerr  
DARPA/NMRO  
1400 Wilson Boulevard  
Arlington, VA 22209-2308

Dr. Max Koontz  
US Dept of Energy/DP 331  
Forrestal Building  
1000 Independence Ave.  
Washington, D.C. 20585

Dr. W. H. K. Lee  
USGS  
Office of Earthquakes, Volcanoes,  
& Engineering  
Branch of Seismology  
345 Middlefield Rd  
Menlo Park, CA 94025

Dr. William Leith  
USGS  
Mail Stop 928  
Reston, VA 22092

Dr. Robert Masse'  
Box 25046, Mail Stop 967  
Denver Federal Center  
Denver, Colorado 80225

K. Morrow  
ACDA/VI  
Room 5741  
320 21st Street N.W  
Washington, D.C. 20451

Dr. Keith K. Nakanishi  
Lawrence Livermore National Laboratory  
P.O. Box 808, L-205  
Livermore, CA 94550 (2 copies)

Dr. Carl Newton  
Los Alamos National Lab.  
P.O. Box 1663  
Mail Stop C335, Group E553  
Los Alamos, NM 87545

Dr. Kenneth H. Olsen  
Los Alamos Scientific Lab.  
Post Office Box 1663  
Los Alamos, NM 87545

Howard J. Patton  
Lawrence Livermore National Laboratory  
P.O. Box 808, L-205  
Livermore, CA 94550

AFOSR/NP  
ATTN: Colonel Jerry J. Perrizo  
Bldg 410  
Bolling AFB, Wash D.C. 20332-6448

HQ AFTAC/TT  
Attn: Dr. Frank F. Pilotte  
Patrick AFB, Florida 32925-6001

Mr. Jack Rachlin  
USGS - Geology, Rm 3 C136  
Mail Stop 928 National Center  
Reston, VA 22092

Robert Reinke  
AFWL/NTESC  
Kirtland AFB, NM 87117-6008

HQ AFTAC/TGR  
Attn Dr. George H. Rothe  
Patrick AFB, Florida 32925-6001

Donald L. Springer  
Lawrence Livermore National Laboratory  
P.O. Box 808, L-205  
Livermore, CA 94550

Dr. Lawrence Turnbull  
OSWR/NED  
Central Intelligence Agency  
CIA, Room 5G48  
Washington, D.C. 20505

Dr. Thomas Weaver  
Los Alamos Scientific Laboratory  
Los Alamos, NM 97544

AFGL/SULL  
Research Library  
Hanscom AFB, MA 01731-5000 (2 copies)

Secretary of the Air Force (SAFRD)  
Washington, DC 20330  
Office of the Secretary Defense  
DDR & E  
Washington, DC 20330

HQ DNA  
ATTN: Technical Library  
Washington, DC 20305

Director, Technical Information  
DARPA  
1400 Wilson Blvd.  
Arlington, VA 22209

AFGL/XO  
Hanscom AFB, MA 01731-5000

AFGL/LW  
Hanscom AFB, MA 01731-5000

DARPA/PM  
1400 Wilson Boulevard  
Arlington, VA 22209

Defense Technical  
Information Center  
Cameron Station  
Alexandria, VA 22314  
( 5 copies)

Defense Intelligence Agency  
Directorate for Scientific &  
Technical Intelligence  
Washington, D.C. 20301

Defense Nuclear Agency/SPSS  
ATTN: Dr. Michael Shore  
6801 Telegraph Road  
Alexandria, VA 22310

AFTAC/CA (STINFO)  
Patrick AFB, FL 32925-6001